Research Article

A Rodent Thyroid-Liver Chip to Capture Thyroid Toxicity on Organ Function Level

Diana Karwelat[1], Julia Kühnlenz[2,3], Thomas Steger-Hartmann[1], Remi Bars[2], Helen Tinwell[2], Uwe Marx[3], Sophie Bauer[3], Oliver Born[4] and Marian Raschke[1]

[1]Pharmaceuticals Division, Investigational Toxicology, Bayer AG, Berlin, Germany; [2]CropScience Division, Toxicology, Bayer S.A.S., Lyon, France; [3]TissUse GmbH, Berlin, Germany; [4]Nuvisan ICB GmbH, Berlin, Germany

Abstract

Endocrine disruption by environmental chemicals continues to be a concern for human safety. The rat, a widely used model organism in toxicology, is very sensitive to chemical-induced thyroid perturbation, e.g., histopathological alterations in thyroid tissue. Species differences in the susceptibility to thyroid perturbation lead to uncertainty in human safety risk assessments. Hazard identification and characterization of chemically induced thyroid perturbation would therefore benefit from *in vitro* models addressing different mechanisms of action in a single functional assay, ideally across species. We here introduce a rat thyroid-liver chip that enables simultaneous identification of direct and indirect (liver-mediated) thyroid perturbation on organ-level functions *in vitro*. A second manuscript describes our work toward a human thyroid-liver chip (Kühnlenz et al., 2022). The presented microfluidic model consisting of primary rat thyroid follicles and liver 3D spheroids maintains a tissue-specific phenotype for up to 21 days. More precisely, the thyroid model exhibits a follicular architecture expressing basolateral and apical markers and secretes T4. Likewise, liver spheroids retain hepatocellular characteristics, e.g., a stable release of albumin and urea, the presence of bile canalicular networks, and the formation of T4-glucuronide. Experiments with reference chemicals demonstrated proficiency to detect direct and indirect mechanisms of thyroid perturbation through decreased thyroid hormone secretion and increased gT4 formation, respectively. Prospectively this rat thyroid-liver chip model, together with its human counterpart, may support a species-specific quantitative *in vitro* to *in vivo* extrapolation to improve a data-driven and evidence-based human safety risk assessment with significant contributions to the 3R principles.

1 Introduction

Disruption of the endocrine system by environmental chemicals continues to be a concern for human health. The biocidal products regulation (BPR) and plant protection products (PPP) regulation demand evidence demonstrating the absence of endocrine-disrupting (ED) potential for human health as part of product registration (EU, 2009, 2012; ECHA et al., 2018; OECD, 2018). Experimentally, the identification of endocrine-disrupting chemicals (EDCs) is based on both *in vitro* and *in vivo* assays. The thyroid gland is one of the main target organs of EDCs. In laboratory animals (mainly rodents), perturbation of thyroid hormone (TH) homeostasis has been shown for several plant protection products (PPPs) (Foster et al., 2021). A chemically-induced impairment of TH homeostasis can induce adverse effects in rodent laboratory animals, such as the formation of thyroid tumors most likely resulting from sustained thyroid stimulating hormone (TSH) stimulation or neurodevelopmental health implications. Indirect (TSH-mediated) neoplastic changes of the thyroid gland in rodents are generally accepted to have little human relevance, acknowledging interspecies differences in the physiology of thyroid hormone homeostasis affecting the vulnerability to perturbation (Meek et al., 2003; Bartsch et al., 2018; Foster et al., 2021). But there are also safety concerns related to a decreased and potentially insufficient supply of TH, especially during pregnancy, with direct health implications for the developing offspring (Noyes et al., 2019; O'Shaughnessy and Gilbert, 2020; Marty et al., 2021). However, evidence of a relevant risk for human health

Received August 26, 2021; Accepted May 27, 2022;
Epub June 21, 2022; © The Authors, 2023.

ALTEX 40(1), 83-102. doi:10.14573/altex.2108262

Correspondence: Diana Karwelat, PhD
Bayer AG
Research & Development, Pharmaceuticals
Investigational Toxicology
Muellerstrasse 178
13353 Berlin, Germany
(diana.karwelat@bayer.com)

is still limited and therefore uncertain (Crivellente et al., 2019). For this reason, TH impairment, induced either by direct or indirect mechanisms, is presumed as human-relevant, particularly in the aspect of maternal thyroid hormone insufficiency (Andersson et al., 2018), in the absence of specific counterevidence. For investigational drugs, such counterevidence can be obtained through the inclusion of relevant parameters in clinical trials; however, such an approach is not amenable to PPPs or industrial chemicals.

Due to their vital importance for metabolic and (neuro-)developmental processes, TH levels are tightly regulated by complex signaling cascades involving several organs. The formation and release of the two THs, thyroxine (T4) and the more active 3,3',5-triiodothyronine (T3), requires stimulation via the hypothalamus-pituitary-thyroid (HPT) axis. The hypothalamus synthesizes and secretes thyrotropin-releasing hormone (TRH), which stimulates the secretion of thyroid-stimulating hormone (TSH) from the anterior pituitary. Upon binding to the TSH receptor (TSHR) on thyrocytes, TSH stimulates the synthesis and release of THs into the circulation. Blood concentrations of THs exceeding the physiological threshold have suppressive activity on the TRH/TSH axis (negative feedback) (Fig. 1). Thyroid growth also occurs subsequently to increased TSH secretion, consequently, prolonged TSH stimulation in response to decreased TH levels leads to pathological changes, e.g., adenoma or tumor formation in rats (Vansell et al., 2004; Brewer et al., 2007; Mullur et al., 2014). In addition, a decline of maternal T4, even in the absence of an accompanying TSH increase (hypothyroxinemia), during vulnerable prenatal periods has been identified as a critical event associated with an increased risk of adverse neurologic outcomes in rats such as hearing loss (ototoxicity) or structural brain malformations (Hassan et al., 2017; Noyes et al., 2019; O'Shaughnessy and Gilbert, 2020; Marty et al., 2021; Gilbert et al., 2022). Interestingly, human epidemiological studies also linked decreased levels of T4 during pregnancy with neurodevelopmental effects in children (Haddow et al., 1999; Kooistra et al., 2006; Berbel et al., 2009; Ghassabian et al., 2014; Modesto et al., 2015; Korevaar et al., 2016; Levie et al., 2018). However, human safety assessments based on experimental data in laboratory animals remain challenging, particularly for PPPs.

The described feedback loop system mirrors a multi-dimensional perturbation potential of chemicals targeting the HPT axis either directly by interfering with the TH production and its control or indirectly by affecting their bioactivity (Sutcliffe and Harvey, 2015) (Fig. 1). Direct mechanisms include interference with key proteins of the thyroid gland such as TSHR, thyroid peroxidase (TPO), or the sodium iodide symporter (NIS) (Santini et al., 2003; Schröder-van der Elst et al., 2004; Beck-Peccoz et al., 2006). Indirect mechanisms, which affect the levels of circulating THs, may include effects on TH transport proteins and the metabolism of THs (Sutcliffe and Harvey, 2015).

The central role of the liver in both the synthesis of the TH-binding proteins albumin, thyroxine-binding globulin (TBG), and transthyretin (TTR) and the catabolism and clearance of THs makes it the primary target organ of indirect thyroid toxicity. As the key metabolizing organ, the liver senses xenobiotics (drugs and environmental chemicals) via the nuclear xenobiotic receptors (XRs). They govern the transcription of drug-metabolizing enzymes (phase I and phase II enzymes) and transporters to facilitate their elimination from the body. Major XRs include the constitutive androgen receptor (CAR), the pregnane X receptor (PXR), the aryl hydrocarbon receptor (AhR), and the peroxisome proliferator-activated receptor (PPAR). Activation of these receptors not only alters the metabolism of xenobiotics through autoinduction but may also enhance TH elimination. Glucuronidation and sulfation are the two main phase II metabolic reactions associated with liver-mediated TH degradation. They are catalyzed by uridine 5'-diphospho-glucuronosyltransferases (UGTs) and sulfotransferases (SULTs), respectively (Peeters and Visser, 2000). Accordingly, XR activation has been determined as one of seven mechanisms of tumor formation in a recently reported adverse outcome pathway network of chemical-induced thyroid activity and remains the most common cause of thyroid cancerogenesis in rodents (ECHA, 2017; Noyes et al., 2019).

While mechanisms of direct thyroid perturbation can be assessed by several validated 2D assays, no standardized test battery is currently available for liver-mediated thyroid toxicity (Paul Friedman et al., 2016; Hallinger et al., 2017; Wang et al., 2018; Noyes et al., 2019). In addition, the widely used 2D *in vitro* assays only capture single molecular initiating events without providing functional readouts, i.e., TH formation and release are not covered. For this reason, animal studies are still required to elucidate the mode of action, determine the specificity of the effect, and eventually extrapolate to the human situation regarding time courses and exposure scenarios (Bergman et al., 2013).

In repeated dose toxicity studies in rodents, long-term elevated TSH, in response to chronic perturbation of thyroid homeostasis, induces thyroid follicular hyperplasia and leads to thyroid follicular adenomas and carcinomas (Capen, 1994; Dybing and Sanner, 1999; Hurley, 1998; Dellarco et al., 2006). However, it is known that rats are considerably more sensitive to TH perturbations than humans due to species differences in the biology, transport, and control of THs. Compared to humans, a shorter

Abbreviations
2D, two-dimensional; 3D, three-dimensional; AE, animal experimentation; AhR, aryl hydrocarbon receptor; AS, animal sacrificed for scientific purposes; ATP, adenosine triphosphate; BPR, biocidal products registration; BNF, β-naphthoflavone; *b*TSH, bovine thyroid-stimulating hormone; cAMP, cyclic adenosine monophosphate; CAR, constitutive androgen receptor; CF, clofibrate; CYP450, cytochrome P450; ECM, extracellular matrix; EDC, endocrine-disrupting chemical; EPA, U.S. Environmental Protection Agency; FC, fold change (treatment response divided by control response); FDA, U.S. Food and Drug Administration; FS, fipronil sulfone; gT4, T4 glucuronide; HPT, hypothalamic–pituitary–thyroid; LC-MS, liquid chromatography-mass spectrometry; LDH, lactate dehydrogenase; MCT8, monocarboxylate transporter 8; MIE, molecular initiating events; MMI, methimazole; MRP2, multidrug resistance-associated protein 2; NIS, sodium iodine symporter; PB, phenobarbital; PCN, pregnenolone-16α-carbonitrile; PPAR, peroxisome proliferator-activated receptor; PPP, plant protection product; PTU, propylthiouracil; PXR, pregnane X receptor; RIF, rifampicin; sT4, T4 sulfate; SULT, sulfotransferase; T3, 3,3',5-triiodothyronine; T4, thyroxine; TBG, thyroid hormone-binding protein; TH, thyroid hormone; TPO, thyroid peroxidase; TSH, thyroid-stimulating hormone; UGT, uridine 5'-diphospho-glucuronosyltransferase; ULA, ultra-low attachment; XR, nuclear xenobiotic receptor; ZO1, zona-occludens-1

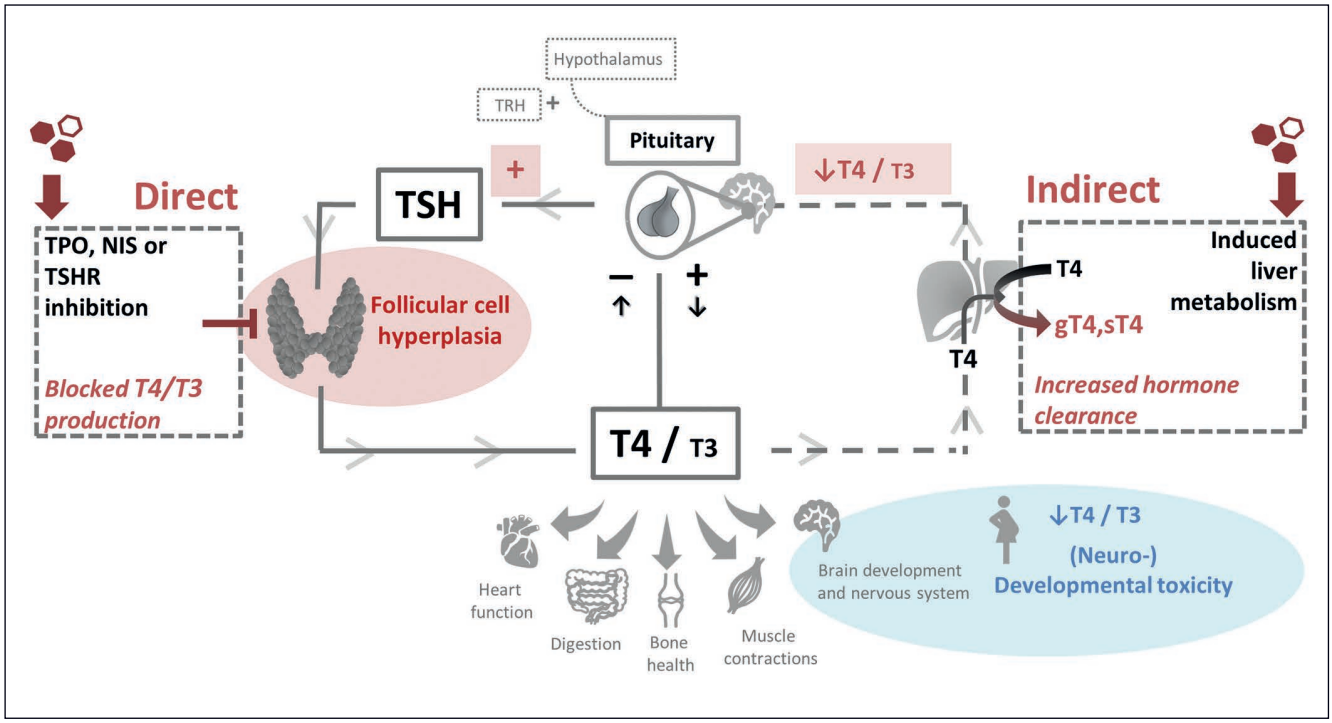

Fig. 1: Schematic presentation of direct as well as indirect mechanisms of thyroid homeostasis perturbation
Thyroid hormone homeostasis is regulated and balanced by the hypothalamus-pituitary-thyroid (HPT) axis. The hypothalamus stimulates the production and secretion of thyroid-stimulating hormone (TSH) from the pituitary gland. The circulatory TSH positively affects the production and secretion of thyroid hormones (TH), which in turn feed back to the hypothalamus-pituitary axis to attenuate TSH secretion. Compounds directly targeting thyroid function (direct mechanisms) lead to the prevention of thyroid hormone production, which results in compensatory elevated TSH levels. Induced hepatic enzyme induction increasing the metabolic clearance of thyroid hormones may also cause a compensatory increase of TSH secretion, referred to as indirect thyroid perturbation. The decline of maternal TH may also implicate adverse effects on brain development and the nervous system in children ((neuro-)developmental toxicity).

TH half-life, as well as a lower binding capacity of the liver-derived TH carrier proteins leads to a reduced TH reserve in rats (Lewandowski et al., 2004; Foster et al., 2021). These species differences significantly limit the value of *in vivo* studies for evidence-based human safety risk assessments. It would therefore be highly desirable to be able to compare direct and indirect mechanisms of thyroid perturbation on a functional level in *in vitro* assays for both species.

Ongoing debates about the necessity and reliability of animal experimentation to assess human safety together with a paradigm shift in toxicology toward an animal-free chemical risk assessment urge the move toward the identification of new approach methodologies (NAMs) (Oredsson et al., 2019; Punt et al., 2020). Organ-on-a-chip (OoC) technologies have greatly enhanced the capabilities to generate and maintain *in vivo*-like microtissues with key functional features and most importantly open novel possibilities to study organ crosstalk by allowing the connection of multiple tissue models (Wikswo, 2014; Kapałczyńska et al., 2018; Raasch et al., 2019). For this reason, they pave the way for complementary approaches and promise an alternative and at the same time ambitious tool for preclinical to clinical translation.

In this manuscript, we demonstrate for the first time a functional chip-based *in vitro* model of the hepatic-thyroid axis with the feasibility to detect direct and indirect thyroid toxicity in the rat. The described concept will enhance the understanding of organ interactions on an *in vitro* level, which is indispensable to initially reduce and ultimately replace animal experiments. However, it has to be pointed out that the established model requires further optimization and qualification before it can be used for regulatory purposes. The model combines primary rat-derived thyroid follicles and liver spheroids utilizing the Chip2 platform. We analyzed structural integrity and organ-specific functionalities for each tissue model separately and in combination. Finally, we successfully tested the utility of the model to detect direct and indirect mechanisms of thyroid perturbation on a functional level.

2 Animals, materials and methods

2.1 Animals

Rat liver cells and thyroid glands were obtained from male Wistar Hannover [Crl:WI(Han)] rats with a weight of 230 to 350 g purchased from Charles River Laboratories (Sulzfeld,

Germany). Animal experimentation was carried out in compliance with EU guidelines and regulations (European and national animal protection laws) and was authorized by the Regional Office for Health and Social Affairs (*LAGeSo*, Berlin, Germany). Briefly, rats were housed in groups on a regular 12-h light/12-h dark cycle. Water and food were available *ad libitum*. Animals were acclimatized for at least one week before experimentation. Hepatocytes and non-parenchymal cells were obtained from rats using a retrograde two-step collagenase perfusion method as described elsewhere (Bale et al., 2016). Briefly, rats were anesthetized by intraperitoneal injection of ketamine-xylazine, the abdomen was opened, and the liver was perfused by cannulation of the portal vein. The first perfusion with a Ca^{2+}-free buffer was followed by a buffer containing Ca^{2+} and collagenase. Subsequently, the liver was excised, placed into a dish containing a basal medium to release the liver cells into suspension, and further processed (see Section 2.6). Afterward, thyroids were excised and further processed (see Section 2.5). Animal experimentation was carried out on 11 animals (further abbreviated as AE – animal experimentation). 18 additional animals were sacrificed for scientific purposes without prior animal experimentation by isofluorane inhalation, followed by the opening of the chest cavity and excision of the thyroid glands (further referred to as AS – animal sacrificed for scientific purposes). Thyroid glands were further processed to establish a thyroid tissue model (see Section 2.5).

2.2 Chemicals

β-Naphthoflavone (Cat#:N3633, CAS#:6051-87-2, ≥ 98%), bovine serum albumin (Cat#:A7096, CAS#:9058-46-8, ≥ 98%), clofibrate (Cat#:41326, CAS#:637-07-0, ≥ 99%), collagenase VII (Cat#:5138), dexamethasone (Cat#:D4902, CAS#:50-02-2), dispase (Cat#:D4693), fetal bovine serum (Cat#:S0615), fipronil sulfone (Cat#:32333, CAS#:120068-36-2), gentamycin (Cat#:G1272), glycyl-L-histidyl-L-lysine (Cat#:CDS020650), Krebs Henseleit buffer (Cat#: K7353), L-thyroxin (Cat#:T1775, CAS#:51-48-9, ≥ 98%), L-thyroxin(-*diphenyl*-$^{13}C_{12}$) (Cat#: 699594, ≥ 98%), methimazole (Cat#:M8506, CAS#:60-56-9, ≥ 99%), phenobarbital (CAS#:50-06-6), pregnenolone 16-α-carbonitrile (Cat#:P0543, CAS#:1434-54-4, ≥ 97%), penicillin-streptomycin (Cat#:P4333), Percoll (Cat#:P4937), 6-propyl-2-thiouracil (Cat#:P3755, CAS#:51-52-5, ≥ 99%), and rifampicin (Cat#:R3501, CAS#:13292-46-1, ≥ 97%) were obtained from Sigma-Aldrich (Milwaukee, Wis., USA). Stock concentrations of β-naphthoflavone, fipronil sulfone, L-thyroxin(-*diphenyl*-$^{13}C_{12}$), methimazole, pregnenolone 16-α-carbonitrile, 6-propyl-2-thiouracil, and rifampicin were dissolved in DMSO at a concentration of 10 mM. Clofibrate and phenobarbital stock concentrations were dissolved in DMSO at a concentration of 1 M. Advanced DMEM/F-12 medium (Cat#:11540446), Glutamax (Cat#:11574466), and collagenase II (Cat#:17101015) were purchased from Thermo Fisher Scientific Inc. (Waltham, USA). Collagen type I purified from rat tail tendons (Cat#:3447-020-01) was purchased from R&D Systems (Minneapolis, USA), sodium iodine (Cat#:134.1, CAS#:7681-82-5, ≥ 99.5%) from Carl Roth GmbH, and native bovine TSH (*b*TSH, Cat#: TSH-1315B) from Creative Biomart. For LC-MS, acetonitrile (ACN), methanol, and acetic acid were purchased from Honeywell (Seelze, Germany). Internal standards (ISTD) of gT4 and sT4 were purchased from Toronto Research Chemicals (Toronto, Canada) and GLSynthech, LLC (Hatfield USA), respectively. Animal-derived components such as FCS, *b*TSH, or rat collagen-I are subject to replacement by animal-free alternatives once these are readily available and fully validated.

2.3 Cell culture media

The liver model was maintained in advanced DMEM/F12 supplemented with 100 nM dexamethasone, 10 ng/mL glycyl-L-histidyl-L-lysine, 2 mM glutamax, 50 µg/mL gentamycin sulfate, 10 U/mL penicillin, and 10 µg/mL streptomycin. Medium for the thyroid follicle culture was additionally supplemented with 100 nM sodium iodine and for stimulation of thyroid hormone synthesis with 5 mIU/mL *b*TSH. Co-culturing was also performed with thyroid follicle culture medium.

2.4 Microfluidic platform

Unless otherwise stated, all cell culture experiments were conducted using the TissUse Multi-Organ-Chip (MOC) platform, the Humimic Chip2 (TissUse GmbH, Germany). One Chip2 comprises two independent microfluidic circuits. Each of these circuits interconnects two individual culture compartments harboring liver and/or thyroid tissue, respectively. An on-chip micropump generates a pulsatile medium flow transporting the medium from one culture compartment to the other and back in a closed loop. The flow rate of the medium is regulated using an external control unit that moves the on-chip micropump membranes by applying pressure air and vacuum at a certain frequency. The control unit was set to a pressure and vacuum of ± 300 mbar and a pumping frequency of 0.45 Hz, which results in an average flow rate of 2.27 µL/min. For a total medium volume of 405 µL used per circuit, this results in a total turnover time of 178 min. Chip2 was incubated for 1-2 days with culture medium before culture of the established models at 37°C and 5% CO_2 in a humidified atmosphere. The morphology of the tissues was monitored every 2-3 days under a light microscope (DMi1, Leica, Wetzlar, Germany).

2.5 Thyroid culture model

For thyroid follicle isolation, thyroids were washed twice with PBS, minced into smaller pieces, and enzymatically digested by incubation in medium containing dispase (2 U/mL) and collagenase II (250 U/mL) for 30-60 min on an orbital shaker at 10 rpm at 37°C and 5% CO_2 in a humidified atmosphere. To separate intact from disrupted follicles and cell debris, the pellet was subsequently allowed to settle naturally. The settled pellet was resuspended carefully in medium containing collagenase IV (100 U/mL), incubated for 1-2 h on an orbital shaker, and monitored regularly for the digestive process. Dissociated follicles were collected by centrifugation at 50 × g and minimized deceleration settings for 10 min, washed with DMEM/F12, and incubated overnight in a T75 ultra-low attachment (ULA) flask (Corning, Arizona, USA) at 37°C and 5% CO_2 in a humidified

atmosphere. On the following day, follicles were counted manually. One rat thyroid gland yielded approximately 800-1100 intact follicles. A total number of 200 follicles were embedded in 100 µL collagen type I gel mix with a final concentration of 2 mg/mL following the manufacturer's instructions. Correspondingly, 100 µL of the follicle-collagen mix was plated per well of a non-treated 24-well cell culture plate (Thermo Fisher Scientific Inc., Waltham, USA) and incubated for 1 h at 37°C for polymerization. Subsequently, 400 µL medium was added to each well leading to a slight detachment of collagen droplets. Using a sterile microspoon (Sigma-Aldrich, Milwaukee, Wis., USA), a single droplet was transferred into the inner compartment of the Chip2 containing 200 µL medium in each compartment and cultured at 37°C and 5% CO_2 in a humidified atmosphere (Fig. 2A). The release of thyroid hormones was stimulated by supplementing the culture medium with 5 mIU/mL *b*TSH. The medium was completely changed (200 µL/compartment) and collected every 2-3 days. The stimulation potency of *b*TSH (5 mIU/mL) was observed by the measurement of cyclic AMP (cAMP) utilizing the cAMP-Glo™ Assay (Cat#:V1501, Promega, Madison, Wisconsin) following the manufacturer's instructions.

2.6 Liver culture model

Hepatocytes, liver endothelial cells, and stellate cells were isolated and purified from rat liver perfusion suspension by percoll density gradient centrifugation. Cell viability was determined by trypan blue exclusion, and isolated cell populations with > 70% viability were used for subsequent spheroid cultures. 96-well ultra-low attachment plates (Thermo Fisher, Nunclon Sphera) were used for self-aggregation and spheroid formation. Briefly, 5000 cells of a mixture of hepatocytes (77.%), stellate cells (10%), and liver-derived endothelial cells (13%) were seeded in 100 µL medium supplemented with 5% FCS per well, centrifuged for 3 min at 50 × g, and incubated at 37°C and 5% CO_2 in a humidified atmosphere for 24 h. Then 50% of the medium volume was renewed, and plates were placed on an orbital shaker at 17 rpm at 37°C and 5% CO_2 in a humidified atmosphere. Initially, 5% FCS was added to achieve optimal spheroid formation. Subsequently, FCS was stripped-off after 3 days by daily partial medium (50%) exchange using serum-free medium for 4 days. FCS supplementation is a common cell culture technique to support primary cell cultures (Baker, 2016), especially during plating. Compact spheroids formed after one week and were collected using wide bore filter tips and embedded in collagen with a final concentration of 2 mg/mL following the manufacturer's instructions. Accordingly, 10 spheroids were pooled, embedded in 100 µL collagen type I solution, and incubated for 1 h at 37°C for polymerization. Thereafter, 100 µL liver culture medium was added to each well leading to a slight detachment of collagen droplets. Using a sterile microspoon, two droplets containing 20 liver spheroids in total were transferred into the outer compartment of the Chip2 and cultured at 37°C and 5% CO_2 in a humidified atmosphere. The medium was completely changed (200 µL/compartment) and collected every 2-3 days (Fig. 3A).

2.7 Co-culture model

The Chip2 circuits were perfused with thyroid culture medium one day before the start of the experiment. On day 1 the medium was renewed (200 µL/compartment), and two droplets of collagen containing 10 spheroids each were transferred to the outer compartment and one droplet with 200 thyroid follicles to the inner compartment of the Chip2 and cultured at 37°C and 5% CO_2 in a humidified atmosphere. For the chosen study design, liver and thyroid culture models were obtained from different animals due to the currently differing pre-culture periods required to set up both tissue models (liver culture model: 7 days vs. thyroid model: 2 days). Further improvements in the long-term stability of the co-culture models at a later timepoint are expected to allow for a fully autologous system with a concomitant reduction in animal demand. The medium was completely changed (200 µL/compartment) and collected every 2-3 days for up to 21 days (Fig. 4A). The viability of the organ models was monitored by measuring lactate dehydrogenase activity (LDH), glucose, and lactate as well as urea and albumin production from the collected supernatants. Collected supernatants were also evaluated for T4 levels via LC-MS.

2.8 Clinical chemistry

Glucose, lactate, and urea concentrations, and lactate dehydrogenase activity (LDH) were measured in culture supernatants using the clinical chemistry analyzer Indiko Plus (Thermo Fisher, Henningsdorf, Germany). Glucose Kit (Cat#:981779, Thermo Fisher), Lactate Kit (Cat#:163000, Thermo Fisher), Urea Kit (Cat#:981820, Thermo Fisher), and LDH Kit (Cat#:981906, Thermo Fisher) were used according to the manufacturer's instructions. Albumin release was quantified using the Rat Albumin ELISA Kit (Cat#:ab235642, Abcam) following the manufacturer's protocol.

2.9 Testing of reference chemicals

Methimazole (MMI) and propylthiouracil (PTU), both thyroid peroxidase (TPO) inhibitors of the thioamide type, were selected as control chemicals directly targeting thyroid function (ECHA, 2021; Singh and Correa, 2021).

The prototypical inducers rifampicin (RIF), pregnenolone 16α-carbonitrile (PCN), fipronil sulfone (FS), β-naphthoflavone (BNF), phenobarbital (PB), and clofibrate (CF) were used to profile the liver culture model for its drug-metabolizing capacity. As substrates of XRs, they induce the expression and activity of enzymes of phase I and II xenobiotic biotransformation, such as cytochrome P450-dependent monooxygenases (CYP450s) and UGTs, *in vitro* and *in vivo*. The administered concentrations were selected based on internal (unpublished) and published data demonstrating induction of the measured CYP450 isoforms or enhanced T4 glucuronidation (Joannard et al., 2000; Klaassen and Hood, 2001; Vansell and Klaassen, 2002; OECD, 2014; Desai et al., 2017; Hariparsad et al., 2017; Dovrtelova et al., 2018; Lu and Di, 2020).

RIF and PCN exhibit specifically different pregnane-X-receptor (PXR) activation profiles. RIF represents a human but not a rat-specific inducer of CYP3A1 (CYP3A1 is the ortholog of the

human CYP3A4). Conversely, PCN has been observed to induce rat but not human CYP3A1 activity (Kocarek et al., 1995). FS was demonstrated to activate CAR and PXR and to induce several CYP phase I enzymes, i.e., rat CYP3A1 activity (Roques et al., 2012, 2013; Caballero et al., 2015). BNF is an AhR ligand and commonly used as a CYP1A1/2 inducer, PB is also known to induce CYP2B3 activity through CAR activation, and CF activates peroxisome proliferator-activated receptor α (PPAR) (Joannard et al., 2000; Ito et al., 2006; Chang et al., 2017).

Inhibition of thyroid hormone synthesis

Thyroid follicle culture was treated for 4 days by adding the fresh compound on culture days 3 and 5. T4 values varied greatly at the beginning of the culture. To increase the likelihood that T4 measurements remained in a quantifiable range, treatment was started on day 3 when the thyroid model secreted higher T4 levels. On day 0 one droplet of collagen containing 100 follicles was transferred in a 96-well plate together with 200 µL medium supplemented with 5 mIU/mL *b*TSH. After 3 days, a concentration series (0.01 µM, 0.1 µM, 1 µM, 5 µM, and 10 µM) of either MMI or PTU dissolved in medium (supplemented with 5 mIU/mL *b*TSH) with a final DMSO concentration of 0.1% was applied and incubated at 37°C and 5% CO_2 in a humidified atmosphere for 48 h. Further, the treatment of medium supplemented with DMSO with a final concentration of 0.1% DMSO served as vehicle control. Subsequently, the complete medium was collected and exchanged with fresh compound for an additional 48 h at 37°C and 5% CO_2 in a humidified atmosphere. Collected supernatants were analyzed for viability markers and T4 levels (via LC-MS). Cellular ATP levels were assessed using the 3D CellTiter-Glo® (Cat#:G9681, Promega, Madison, Wisconsin) assay according to the manufacturer's instructions. Briefly, one collagen droplet containing 100 follicles was transferred to a 96-well plate and 100 µL CellTiter-Glo® reagent and 100 µL medium were added. Luminescence was measured using a microplate reader (SynergyNeo2, BioTek Instruments, Vermont, USA).

For data analysis, technical replicates were normalized to the mean of DMSO solvent controls, and mean normalized values were plotted independently for each experiment for T4 as well as ATP levels.

Induction of liver biotransformation

The liver model was treated for 6 days with fresh compound added after 3 days. Briefly, the Chip2 circuits were perfused with liver culture medium one day before the start of the experiment. On day 1, the medium was renewed (200 µL/compartment), and two collagen droplets containing 20 spheroids were transferred to one compartment. Next day (day 0), the medium was removed, and medium containing either vehicle control (0.1% DMSO), 10 µM RIF, 10 µM PCN, 10 µM FS, 10 µM BNF, 1 mM PB, or 1 mM CF supplemented with 1 µM L-thyroxine was administered and incubated for 72 h at 37°C and 5% CO_2 in a humidified atmosphere. Culture supernatants were collected and exchanged for media containing fresh compounds followed by incubation for an additional 72 h at 37°C and 5% CO_2 in a humidified atmosphere. Subsequently, liver spheroids were evaluated for CYP450 activity. Collected culture supernatants were analyzed for the levels of T4 glucuronide (gT4) via LC-MS.

For data analysis, technical replicates were normalized to the mean of DMSO solvent controls, and mean normalized values were plotted independently for each experiment for CYP450 activity as well as gT4 levels.

Combined testing in the co-culture setup

Reference chemicals were incubated as described above with supplementation of 1 µM L-thyroxine-diphenyl-$^{13}C_{12}$ to allow differentiation of *de novo* synthesized T4 from supplemented L-thyroxine. Collected supernatants were analyzed for viability markers, T4 levels, and labeled L-thyroxine glucuronide formation (gT4►) by LC-MS.

2.10 Analysis of thyroid hormones and metabolites by LC-MS

Thyroid hormones (TH; T4 and T3) and T4 metabolites (gT4, sT4) were measured using the Quadrupole LC/MS/MS mass spectrometer Triple Quad 5500 (AB Sciex Instruments, Framingham, USA). For each sample, 100 µL of conditioned medium was combined with 400 µL of an internal standard mixture (ACN/H_2O/ISTD) in a 96-well polypropylene deep well plate and centrifuged (15 min, 1800 x g). 300 µL of the supernatant was transferred, dried under nitrogen, and reconstituted with 100 µL methanol/water (50/50) for analysis. For ultra-high-performance liquid chromatography, a sample volume of 10 µL was injected into the analytical column (Acquity UPLC BEH C18 1.7 µm, 2.1 x 50 mm). A linear gradient using 0.1% acetic acid in water as mobile phase A and 0.1% acetic acid in methanol as mobile phase B was used at a flow rate of 0.6 mL/min. Gradient elution was performed using water (mobile phase A) and methanol (mobile phase B) at a flow rate of 0.6 mL/min. The starting composition was 95% mobile phase A and 5% mobile phase B. After 1 min, the gradient was ramped to 95% mobile phase B and held for 1 min. The column was re-equilibrated to starting conditions for 1 min. THs were detected by multiple reaction monitoring in negative electrospray ionization mode operated with an Ion Turbo Spray source. The source parameters were 35 psi for the curtain gas, -4500 kV for the ion spray voltage, 650°C for the source temperature, 60 psi for gas 1, and 80 psi for gas 2. The declustering potential (DP), collision energy (CE), and cell exit potential (CXP) were optimized at 135 V, 130 V, 11 V for L-thyroxine (T4), 140 V, 130 V, 9 V for the labeled T4, 155 V, 78 V, 9 V for triiodothyronine (T3), 115 V, 130 V, 11 V for T4 glucuronide (gT4), and 15 V, 36 V, 21 V for T4 sulfate (sT4). Maximum sensitivity was achieved by optimizing each analyte separately using the Analyst software v.1.6.3 (AB Sciex Instruments, Framingham, USA). The lower limit of quantification was 0.001 µM for T3 and sT4 and 0.005 µM for T4 and gT4.

2.11 Cytochrome P-450 activity

Enzyme activities of CYP3A1, CYP1A2, CYP2B3, and CYP4A2 in rat liver spheroids were determined by using

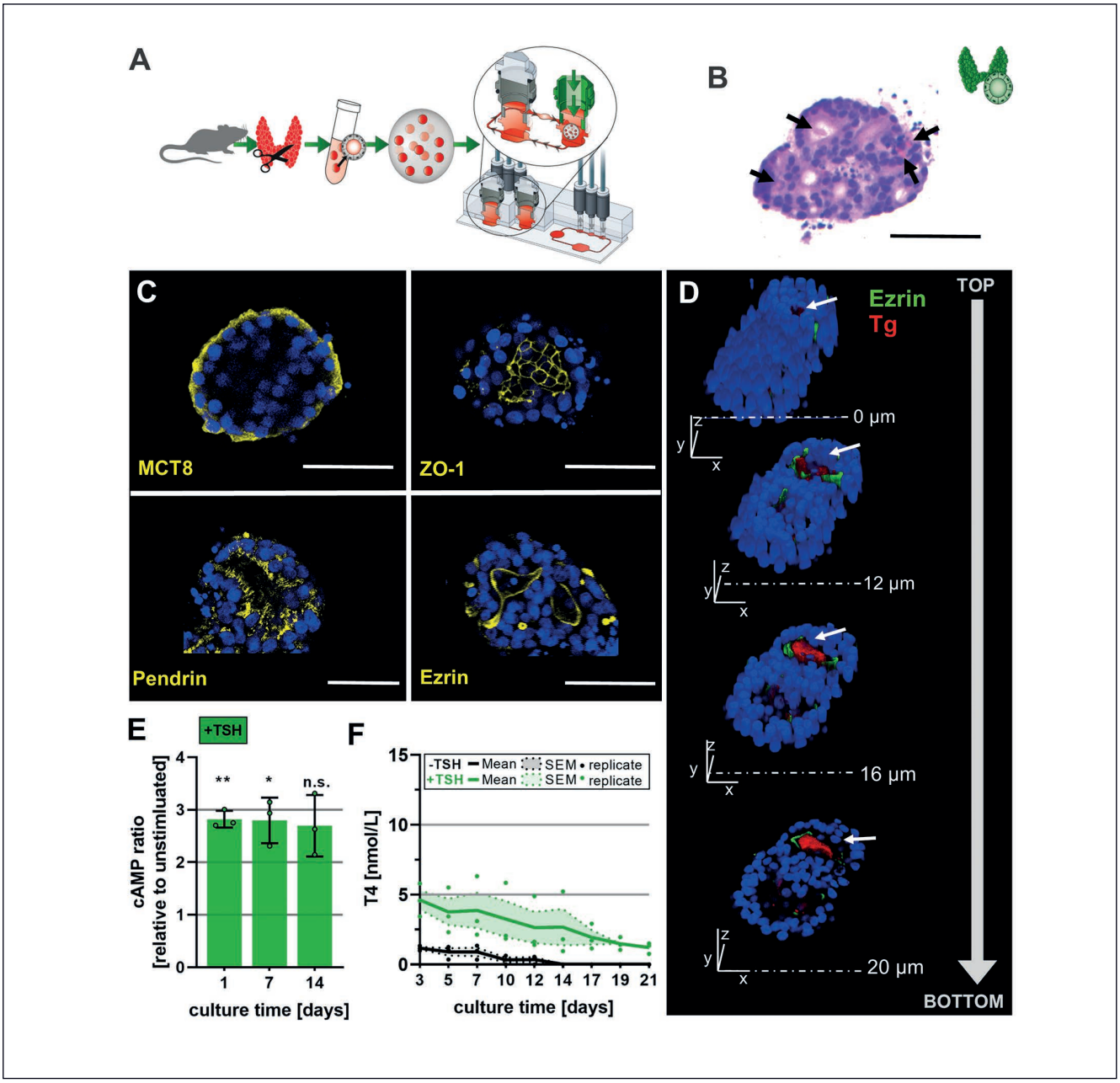

Fig. 2: Thyroid follicles preserve the specialized follicular architecture and display TSH-dependent thyroid hormone production
(A) Schematic representation of the 3D thyroid culture model. Thyroid follicles were enzymatically dissociated, embedded in collagen, and cultured in the Chip2. (B) H&E-stained sections (5 μm thick) of primary thyroid follicles after 14 days in culture. Pink stained colloid (marked with arrows) and cell nuclei stained with hematoxylin in blue. The scale bar is 50 μm. (C) Thyroid follicles cultured for at least 14 days (in the presence of *b*TSH) and immunohistochemically stained for monocarboxylate transporter 8 (MCT8), pendrin, tight junction zonula occludens-1 (ZO-1), and ezrin in yellow; cell nuclei stained with Hoechst 33342 in blue. Merged projection images of z-planes (z = 10-30 μm). The scale bar is 50 μm. (D) 3D panel presentation from the top to the bottom view of a thyroid follicle immunohistochemically stained for ezrin in green and thyroglobulin (Tg) in red; cell nuclei stained with Hoechst 33342 in blue. The scale bar is 50 μm. (B-D) Representative images of n = 3. (E) cAMP production in response to 5 mIU/mL *b*TSH on day 1, 7 and 14. Data are shown as a ratio relative to non-stimulated follicles (mean ± SD) of 3 independent experiments with cells from 1 animal (AE) per experiment with 2 technical replicates per experiment (n = 3). (F) T4 levels quantified from culture supernatants of thyroid follicles cultured for 21 days in the absence (black) or presence (green) of 5 mIU/mL *b*TSH. T4 levels were measured via LC-MS and presented as mean ± SD (dotted line) of 3 independent experiments with cells from 1 animal (AE) per experiment with 2 technical replicates per experiment (n = 3). Statistics were performed by two-way ANOVA with Dunnett's correction for multiple comparison tests with *, $p < 0.001$ versus vehicle control.

P450-Glo™ Assay Kits (CYP3A1 Cat#:V9002, CYP1A2 Cat#:V8771, CYP2B3 Cat#:V8321, CYP4A2 Cat#:V8887; Promega, Madison, Wisconsin) according to the manufacturer's instructions. CYP3A1 activity was evaluated for liver spheroids treated with RIF, PCN, or FS and the vehicle control. CYP1A2, CYP2B3, and CYP4A2 activities were analyzed after treatment with BNF, PB, and CF, respectively, as well as with the vehicle control. Following treatment with reference chemicals, 10 collagen-embedded liver spheroids were transferred to a 96-well plate and washed with PBS. CYP3A1 substrate was diluted in medium, and 100 µL of substrate solution was added to the collagen-embedded spheroids and incubated for 4 h. CYP1A2, 2B6, and 4A2 substrates were diluted in Krebs-Henseleit buffer supplemented with 3 mM salicylamide. 100 µL of substrate solution was added to the collagen-embedded spheroids followed by an incubation period of 18 h. Subsequently, 75 µL of the culture supernatants were incubated with equal amounts of detection reagent for 20 min at room temperature, and luminescence was measured using a microplate reader (SynergyNeo2, BioTek Instruments, Vermont, USA). Relative luminescence signals were normalized to the vehicle controls.

2.12 Histological and immunohistochemical staining

Collagen-embedded 3D culture models were washed in PBS, fixed in 4% paraformaldehyde (PFA) followed by routine histological processing and finally paraffin wax embedding. 5 µm sections were cut and stained with haematoxylin and eosin (H&E). Images were taken with a Leica DMI8 microscope and DFC450C camera using a 20 × objective (HC PL FLUOTAR L 20x/, NA 0.4). Images were processed with the Leica Application Suite X software.

For immunofluorescence staining, embedded culture models were transferred into a 1.5 mL tube, washed three times with PBS, and fixed in 4% PFA for 30-45 min. Thyroid follicles and liver spheroids were incubated in permeabilization buffer (0.25% Triton X-100 and 0.25% Tween 20 in PBS) for 20 min or 4-6 h respectively. Droplets were washed three times with wash buffer (0.001% Triton X-100 in PBS) and blocked overnight at 4°C in PBS containing 10% BSA. Primary antibodies were used against ZO-1 (Invitrogen Cat#:61-7300, RRID:AB_2533938), albumin (Abcam Cat#:ab207327, RRID: AB_2755031), MCT8 (Atlas Antibodies Cat#:HPA003353, RRID: AB_1079343), pendrin (Novus Cat#:NBP1-85237, RRID: AB_11032075), and ezrin (Thermo Fisher Scientific Cat#:PA5-82769, RRID: AB_2789925) diluted 1:50 in PBS containing 3% BSA. Primary antibodies against MRP2 (Enzo Life Sciences Cat#: ALX-801-016-C250, RRID: AB_2051908) and thyroglobulin (Biotium Cat#:BNC40023, RRID: AB_2891021) were diluted 1:20 and 1:100 respectively in PBS containing 3% BSA. Diluted primary antibodies were incubated at 4°C overnight. As secondary antibodies, goat anti-rabbit (Biotium Cat#:20012, RRID: AB_10559670) conjugated to CF488 or goat anti-mouse (Biotium Cat#:20110, RRID: AB_10557031) conjugated to CF594 were diluted 1:1000 in wash buffer and incubated for 1 h. Nuclei were counterstained with Hoechst 33342 (Invitrogen, Cat#:H3570). None of the used antibodies were obtained from ascites fluids (as confirmed by suppliers). For image acquisition, organ models were placed in a wash buffer or cleared with a 3D clearing reagent (Abcam, Cat#:ab243302). Images were taken with a Leica SPE8 confocal microscope and DCF7000T camera using a 20 x objective (ACS APO, NA 0.6) and 40 x objective (HC PL APO CS2, NA 1.1). Images were processed with the Leica Application Suite X software.

2.13 Statistical analysis

GraphPad Prism (GraphPad Software v. 8.0.2., Inc., San Diego, CA) was used for analysis. A one-way ANOVA with Dunnett's correction for multiple comparisons was performed to analyze the effect of *b*TSH on cAMP levels in thyroid culture. Likewise, concentration-dependent effects of MMI or PTU on T4 were analyzed. Two-way ANOVA followed by a Sidak comparison was performed to analyze the time-dependent effects of MMI or PTU. IC50 values for MMI or PTU treatment were calculated using a non-linear fit sigmoidal dose-response curve (log [inhibitor] versus relative T4 levels). The effect of prototypical liver inducers on CYP activity and gT4 formation was analyzed by an unpaired t-test with correction for multiple comparisons with the Holm-Sidak method. P-values < 0.05 were considered statistically significant.

3 Results

3.1 Thyroid follicles pose TSH-dependent thyroid hormone biosynthesis

In a first step, a viable thyroid follicle culture was established and characterized. For this purpose, primary rat thyroid follicles were isolated from fresh thyroid tissue, embedded in a collagen I matrix, and cultivated in the Chip2 (Fig. 2A). Morphology and the ability to produce THs were analyzed. Brightfield microscopy indicated the successful isolation of closed, oval-shaped follicles (Fig. S1A[1]). After 14 days in culture (in the presence of *b*TSH), H&E staining demonstrated the thyroid follicle-specific lumen with eosinophilic colloid (indicated by arrows), surrounded by a layer of epithelial cells (thyrocytes) (Fig. 2B). Confocal microscopy of immunostained follicles confirmed correct apicobasal thyrocyte polarity with a basolateral expression of monocarboxylate transporter 8 (MCT8), responsible for the basolateral transport of THs, and apical expression of the iodine exchange protein pendrin. The expression of the distinct tight junction associated protein zonula occludens-1 (ZO-1) and the cytovillin ezrin also indicated a defined cellular organizational structure (Fig. 2C).

[1] doi:10.14573/altex.2108262s

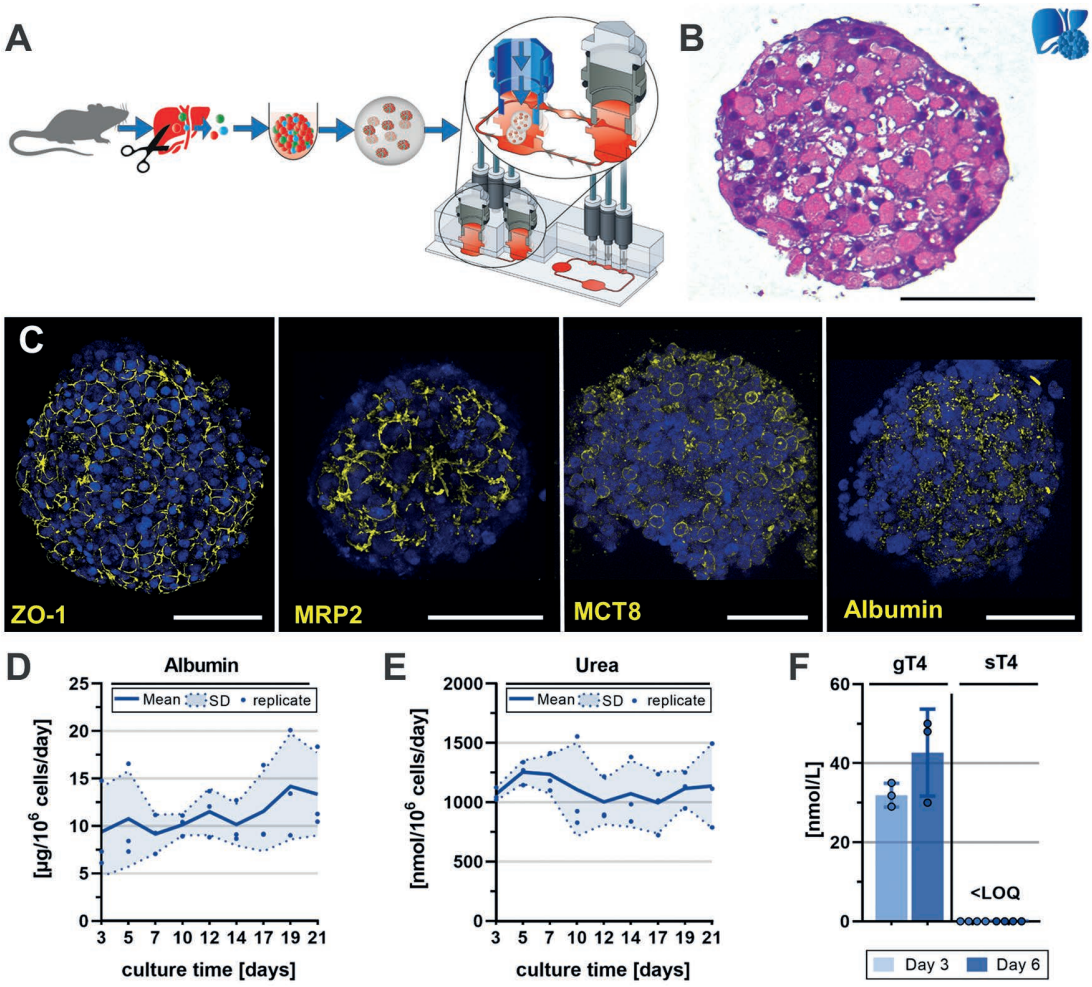

Fig. 3: Liver spheroids retain hepatocellular polarity and liver-specific functionality

(A) Schematic representation of the liver spheroid culture model. Hepatocytes and non-parenchymal cells were isolated from rats, spheroids were formed in ULA plates, embedded in collagen, and cultured in the Chip2. (B) H&E sections (5 μm thick) of a primary rat liver spheroid after 14 days in culture. The scale bar is 100 μm. (C) Liver spheroids were cultured for at least 14 days and immunohistochemically stained for tight junction zonula occludens-1 (ZO-1), albumin, monocarboxylate transporter 8 (MCT8), and the multidrug resistance-associated protein 2 (MRP2) in yellow; cell nuclei stained with Hoechst 33342 in blue. Merged projection images of z-planes (z = 40-60 μm). The scale bar is 100 μm. (D) Albumin and (E) urea production was quantified in culture supernatants over 21 days. Data presented as mean ± SD (dotted line) of 3 independent experiments with 2 technical replicates from 1 animal per experiment (n = 3). (F) T4 glucuronide (gT4) and sulfate (sT4) formation of liver spheroids incubated with 1 μM L-thyroxine for 72 h. Data presented as mean ± SD of 3 independent experiments with 2 technical replicates from 1 animal (AE) per experiment (n = 3).

Furthermore, immunostaining demonstrated the presence of the essential TH precursor protein thyroglobulin in the follicle lumen, enclosed by the cytovillin marker ezrin (Fig. 2D). The TSH-dependent increase of cAMP production for at least 14 days verified the responsiveness of the thyroid model towards *b*TSH (Fig. 2E). Similarly, gene expression analysis demonstrated stable stimulatory upregulation of TSH-dependent genes like *Tpo* and *Nis* (Fig. S1B[1]). Monitored viability markers (lactate levels, glucose consumption, and lactate dehydrogenase release) showed increased energy metabolism upon *b*TSH stimulation (Fig. S1C[1]). To confirm relevant thyroid function, TH levels in culture supernatants were measured via LC-MS over 21 days. In the presence of *b*TSH, thyroid follicles produced levels of

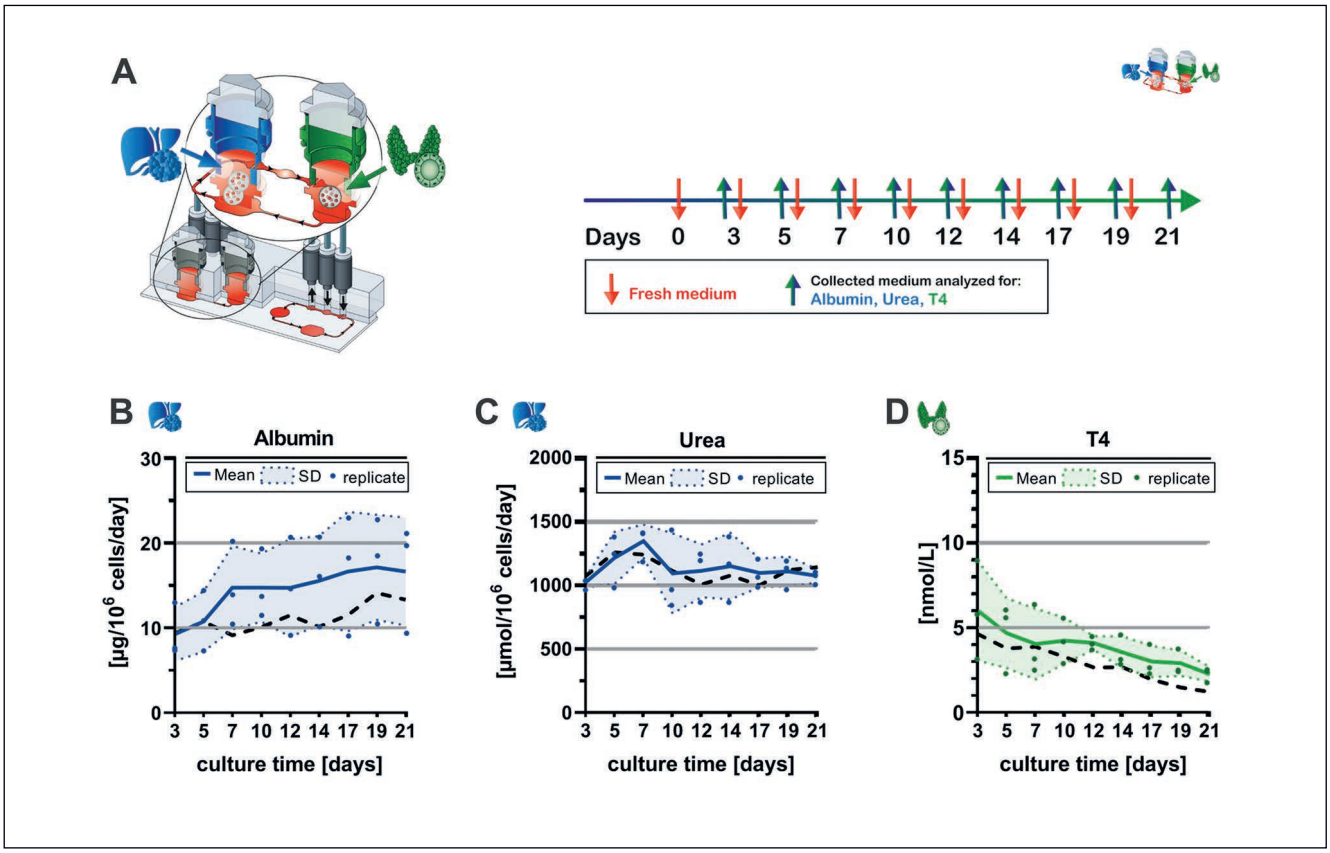

Fig. 4: Thyroid-liver co-cultivation remains viable and functional

(A) Schematic presentation of liver-thyroid co-culture setup. Embedded liver spheroids and thyroid follicles were co-cultured over 21 days in the presence of *b*TSH. Medium collection and replacement was performed every 2-3 days. (B) Albumin and (C) urea production was quantified in culture supernatants over 21 days. (D) T4 concentrations were measured via LC-MS in medium supernatants over 21 days in the presence of 5 mIU/mL *b*TSH. Data presented as mean ± SD (dotted line) of 3 independent experiments with 2 technical replicates with liver cells obtained from 1 animal per experiment (AE) and thyroid cells obtained from 1 different animal (AS) per experiment (n = 3). The black dashed line presents the same mean values of Fig. 3D, E of single liver cultures, and Fig. 2F of single thyroid cultures.

1-6 nmol/L of the dominant thyroid hormone T4. Levels decreased slightly over time but were clearly above those of unstimulated culture models (Fig. 2F).

Together, these data demonstrate key morphological and functional properties of thyroid follicles with the capacity to produce T4 upon TSH stimulation.

3.2 Liver spheroids retain hepatocellular polarity and key functional features

The liver model was composed of primary liver spheroids generated from freshly isolated primary rat hepatocytes and NPCs embedded in a collagen gel. These collagen-embedded liver spheroids were transferred to the Chip2 and maintained for up to 21 days (Fig. S2A[1], Fig. 3A). All spheroids remained relatively uniform in shape for the culture period (Fig. S2B[1]). Morphological and functional features such as liver-specific protein expression and secretion as well as metabolic activities were assessed. After 14 days in culture, liver spheroids demonstrated a compact cellular arrangement in H&E staining along with intact cell-cell contacts and the formation of a bile canaliculi-like network, evident from immunostaining of the tight-junction marker ZO-1 and the apical export multi-drug-protein 2 (MRP2), respectively (Fig. 3B,C). Expression of the TH transporter protein MCT8 and albumin was also confirmed (Fig. 3C). Further, single cultures of liver spheroids demonstrated stable secretion of the hepatic markers albumin and urea for at least 21 days of culture, with concentrations ranging from 7.5-13.0 µg albumin/10^6 cells/day (Fig. 3D) and 750-1,500 nmol urea/10^6 cells/day (Fig. 3E). Additionally, monitored viability parameters (lactate, glucose, LDH) as well as analyzed gene expression evinced stable functional liver spheroids for at least 14 days (Fig. S2C,D[1]). T4 catabolism by hepatic UGT and SULT was determined by quantification of T4 glucuronide and sulfate formation (gT4, sT4 respectively) following supplementation of 1 µM L-thyroxine for 72 h. Liver-mediated T4 conjugation was monitored for up to 6 days to enable subsequent experiments with prototypic in-

ducers of liver biotransformation (see Section 2.9). Accordingly, liver spheroids exhibited UGT activity with gT4 concentrations ranging between 35 and 50 nmol/L. In contrast, sT4 was not detectable in medium supernatants, suggesting that rodent liver spheroids possess no or only little capacity to metabolize T4 via sulfotransferases (Fig. 3F).

Taken together, this data demonstrates that the established liver model maintains hepatocellular polarity and functionality, and most importantly, the baseline activity of UGT to conjugate T4.

3.3 Co-culture of the thyroid and liver model is a viable and functional model

Following the approach of a liver-thyroid co-culture, embedded liver spheroids and thyroid follicles were transferred to the Chip2 and cultured under *b*TSH supplementation for 21 days (Fig. 4A). The medium was replaced every 2-3 days, collected, and analyzed for the liver-specific markers albumin and urea, and T4 released from the thyroid model. Albumin and urea secretion from the liver spheroids remained largely constant for 21 days and similar to that of single liver cultures (Fig. 4B-D, dashed line), with medium concentrations ranging between ca. 9-15 µg/10^6 cells/day (Fig. 4B) and ca. 750-1,500 nmol/10^6 cells/day, respectively. T4 levels released from the thyroid models initially reached 6 nmol/L but declined to ~ 2 nM after 14 days (Fig. 4D). In comparison to the single culture, the combination of both tissues evinced higher viability markers (lactate, glucose consumption, LDH) and a robust gene expression profile (Fig. S3B,C[1]).

These results demonstrate that a thyroid-liver co-culture model in the Chip2 is viable and allows both tissues to maintain important phenotypic functions.

3.4 Thyroperoxidase (TPO) inhibitors diminish T4 secretion

To investigate the utility of the thyroid model in identifying compounds that directly affect thyroid function, the two TPO inhibitors methimazole (MMI) and 6-propylthiouracil (PTU) were administered at selected concentrations ranging from 0.01-10 µM starting on culture day 3 with repeated treatments every second day for the next 4 days (Fig. 5A,B). Treatment with MMI or PTU did not affect the cell viability readout ATP but induced a clear and concentration-dependent reduction of T4 in the culture supernatant with IC50 values of 0.562 µM (MMI) and 0.406 µM (PTU) (Fig. 5C,E). T4 medium levels already significantly declined two days after a single treatment with 10 µM MMI to 2-5 nmol/L compared to 7-10 nmol/L in vehicle controls (Fig. 5D). Also, a single treatment with 10 µM PTU resulted in a significant decrease in T4 medium levels (Fig. 5F). Further experiments conducted under microfluidic conditions also demonstrated a concentration-dependent T4 reduction by MMI and PTU (Fig. S4[1]).

These data show that the established thyroid culture model is synthesizing and secreting THs in a TSH-dependent manner and allows detection of direct thyroid toxicity on a functional level, i.e., TH release.

3.5 Known inducers of liver biotransformation enhance T4 catabolism in the liver model

The metabolic capacity of the liver model as well as its utility to detect indirect thyroid perturbation through increased thyroid hormone catabolism were evaluated by determination of CYP450 enzyme activity and gT4 formation following treatment with prototypical inducers. These compounds are substrates of the XRs CAR, PXR, AhR, and PPARα (see Fig. 6B) and well-established positive controls in screening experiments for liver induction. RIF, PCN, FS, BNF, PB, and CF were administered every 3 days for 6 days in the presence of 1 µM L-thyroxine (Fig. 6A,B). All tested compounds induced characteristic patterns of CYP450 isoenzyme induction. Accordingly, RIF treatment showed no effect on CYP3A activity. The well-known CYP3A1 inducers PCN and FS promoted a significantly higher induction (2.6 and 2.4-fold induction respectively) compared to the vehicle control. When treated with BNF, CYP1A2 activity was significantly induced 13.6-fold. Additionally, PB and CF significantly enhanced CYP2B3 and CYP4A11 enzyme activity, respectively (Fig. 6C).

Treatment with RIF did not affect the amount of gT4 whereas all other tested compounds significantly increased the gT4 levels in the culture medium compared to the vehicle control. The highest fold change was determined for PCN with a 2.7- and 2.8-fold increase after 3 days and 6 days of treatment, respectively (Fig. 6D).

These data demonstrate that the established liver model possesses baseline metabolic activity and inductive capacity to detect treatment-related induction of CYP450-isoenzymes and T4 catabolism.

3.6 Co-cultivation demonstrates the possibility of concomitantly deciphering direct and indirect thyroid effects in a single *in vitro* approach

Preliminary results indicated that the analysis of hepatic phase II detoxification (T4 glucuronidation) requires T4 concentrations that exceed the capacity of the thyroid *in vitro* model. Supplementation of labeled L-thyroxine facilitates sensing of gT4 formation as well as T4 production concomitantly. To test the functionality concerning direct and indirect perturbation scenarios, the co-culture was exposed to previously tested compounds (see Section 2.9) (Fig. S5A,C[1]).

The effects of the TPO inhibitors MMI or PTU on TH levels as well as gT4 formation (labeled L-thyroxine glucuronide) in co-culture were investigated. The exposure regimen was identical to the single culture treatment (see Section 3.1) but only a low (0.1 µM) and a high (10 µM) concentration of MMI or PTU were applied (Fig. S5A1). Correspondingly, the exposure of both concentrations showed no effect on thyroid or liver cell viability (Fig. 7AI,II). Basal T4 levels (CTRL) ranged between 1-4 nmol/L and diminished in response to MMI or PTU treatment in a time- and concentration-dependent manner (Fig. S5C[1]). Thus, low exposure concentrations only moderately inhibited T4 levels by about 10-20%, but high exposure concentrations induced a clear reduction of T4 by 80% and 70% after 4 days

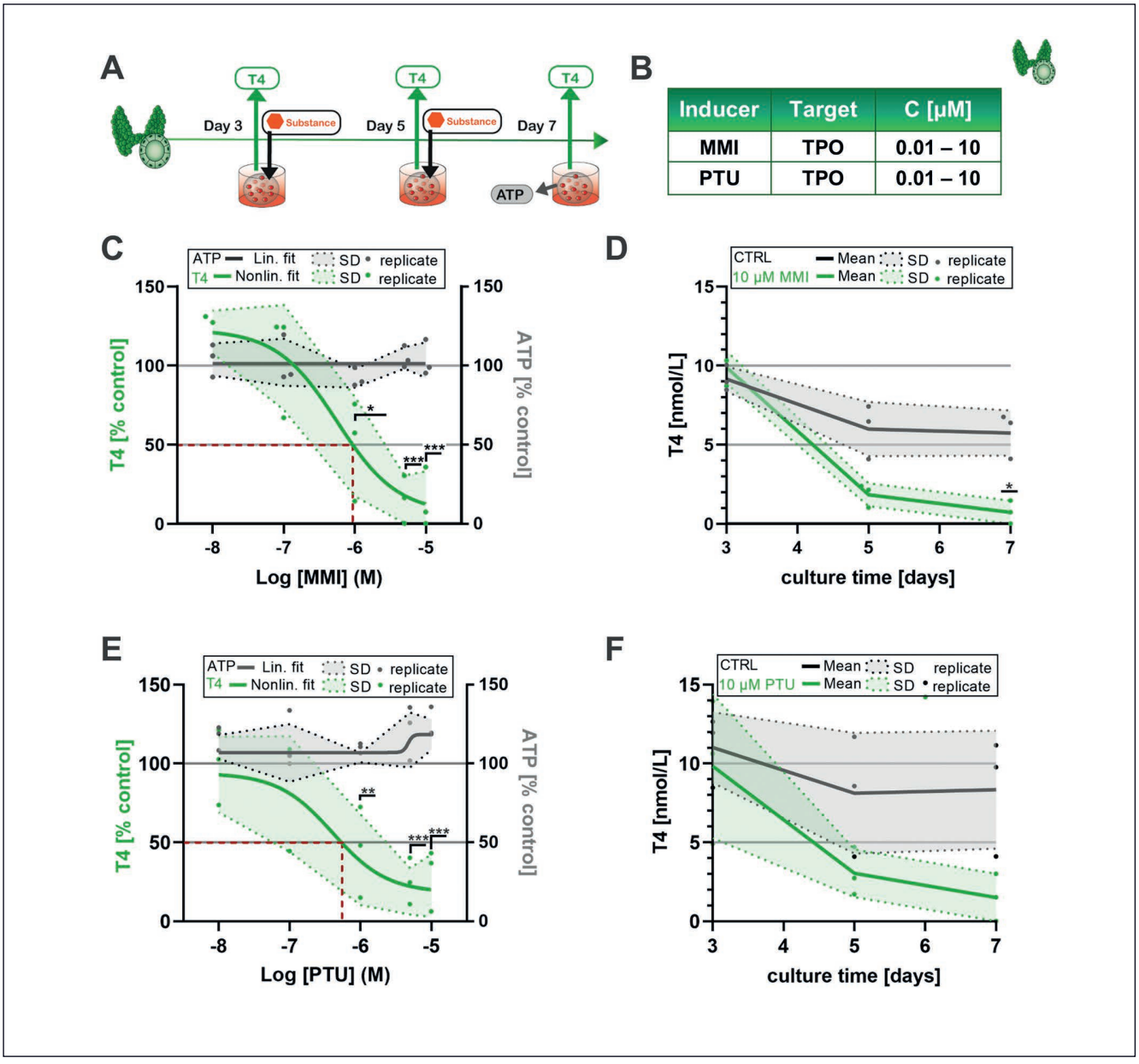

Fig. 5: TPO inhibitors diminish thyroid T4 production

(A) Schematic representation of TPO inhibitor treatment regimen. After 3 days in culture, the thyroid culture model was treated for 4 days with fresh compound added on day 3 and day 5. Culture supernatants were analyzed for T4 on day 3, 5, and 7. ATP levels were measured after 4 days of treatment (day 7 in culture). (B) Chemicals with enzyme inhibitory mechanisms were selected as a reference set of compounds disrupting thyroid hormone secretion (methimazole (MMI) and 6-propyl-2-thiouracil (PTU)). Specifications for chemical name, target enzyme, and utilized concentrations are noted. (C) T4 (green) and ATP (black) levels in % relative to vehicle control (DMSO) after 4 days of treatment with different concentrations (0.01 μM, 0.1 μM, 1 μM, 5 μM, and 10 μM) of MMI. Data fitted by a non-linear fitted regression line ([agonist] vs. response-variable slope (four parameters)). (D) T4 concentration over time after treatment with 10 μM MMI (green) or vehicle control (DMSO, black). (E) T4 (green) and ATP (black) levels in % relative to vehicle control (DMSO) after 4 days of treatment with different concentrations (0.01 μM, 0.1 μM, 1 μM, 5 μM, and 10 μM) of PTU. Data fitted by a non-linear fitted regression line ([agonist] vs. response-variable slope (four parameters)). (F) T4 concentration over time of treatment with 10 μM PTU (green) or vehicle control (DMSO, black). All data presented as mean ± SD (dotted line) of 3 independent experiments with 2 technical replicates from 3 animals (3 AS, 3 AE) per experiment (n = 3). Statistics were performed by two-way ANOVA with Dunnett's correction for multiple comparison test with *, $p < 0.033$; **, $p < 0.0052$; ***, $p < 0.001$ versus vehicle control.

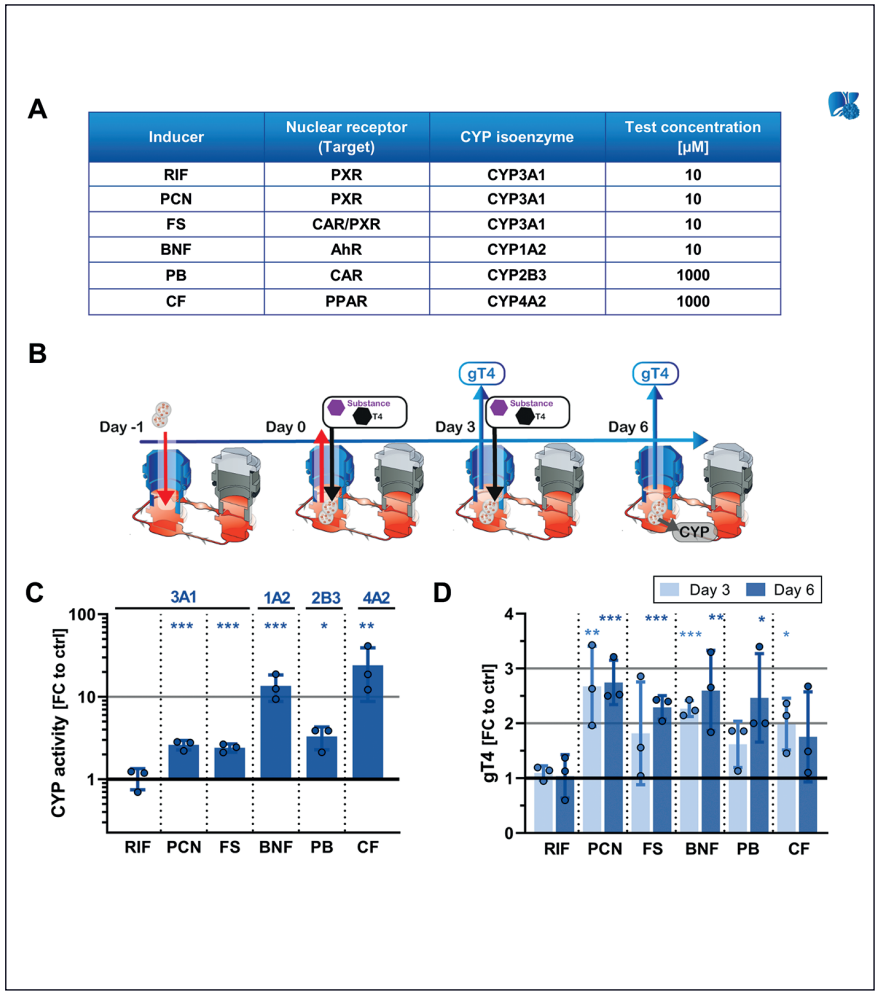

Fig. 6: Prototypical liver metabolism inducers enhance CYP450 activity and T4 catabolism

(A) Overview of the set of liver-inducing reference compounds: rifampicin (RIF), pregnenolone 16-α-carbonitrile (PCN), fipronil sulfone (FS), β-naphthoflavone (BNF), phenobarbital (PB) and clofibrate (CF) listed with the targeted nuclear receptor, most efficiently induced CYP450 isoforms, and the test concentrations used in this study. (B) Schematic presentation of liver spheroid treatment regimen in the Chip2. Liver spheroids were treated on day 0 and 3. The medium was supplemented with 1 μM T4. Culture supernatants were analyzed for gT4 formation on day 3 and 6. CYP450 activity was measured after 6 days of treatment. (C) The fold-induction of CYP450 isozyme activity after 6 days of treatment with inducers (3A1: RIF, PCN, FS; 1A2: BNF; 2B3: PB; 4A2: CF) and (D) gT4 formation after 3 and 6 days of treatment relative to vehicle control (DMSO). Data presented as mean ± SD of 3 independent experiments with 2 technical replicates obtained from 1 animal (AE) per experiment (n = 3). Statistical significance determined using the Holm-Sidak t-test (α = 0.05) with $^{*}p < 0.005$, $^{**}p < 0.005$ and $^{***}p < 0.0001$ versus corresponding control.

of MMI or PTU treatment, respectively. The inhibitor-related effects were only observed for thyroid function; thus liver biotransformation was not affected at any timepoint as demonstrated by consistent liver-mediated gT4 formation (Fig. 7AII, Fig. S5B[1]).

Furthermore, inducers of liver biotransformation (see Section 3.2) were added to the co-culture and T4 levels and liver metabolism (CYP450 enzyme induction, gT4▶ formation) were analyzed (Fig. S5D[1]). The viability of thyroid follicles was not affected by the compounds, and basal T4 levels ranged between 4-6 nmol/L (Fig. 7BI, Fig. S5E[1]). These levels were slightly reduced by 10-30% in response to FS, BNF, PB, or CF exposure (Fig. 7BI). However, the observed liver induction pattern was consistent with the pattern observed from single-culture treatments. Consequently, the potent human but not rat inducer RIF showed neither an effect on CYP450 activity nor gT4▶ formation. However, PCN, FS, BNF, PB, and CF promoted elevated CYP450 activities and gT4▶ levels (Fig. 7CII, Fig. S5F[1]). Of note, the highest fold change of gT4▶ formation was observed for BNF with an approximately 3-fold increase after 3 and 6 days of treatment (Fig. 7BII).

Taken together, this co-culture model allowed the functional and species-specific assessment of liver-mediated gT4▶ formation and simultaneous quantification of T4 despite labeled L-thyroxin supplementation. Most importantly, these results demonstrate the ability of the liver-thyroid co-culture to assess direct thyroid effects at the functional level while ruling out indirect (liver-mediated) effects and *vice versa*.

4 Discussion

Systemic toxicity testing in rodents still represents a mandatory regulatory requirement for the human safety risk assessment of compound classes such as PPP and industrial chemicals. The evaluation of the human relevance of adverse effects observed in animal assays is a major challenge in several areas of toxicology, including thyroid disruption. Rodents are particularly sensitive to perturbations of thyroid homeostasis. Perturbations may arise from direct interference of compounds with the thyroid gland or through indirect, predominantly liver-mediated mechanisms.

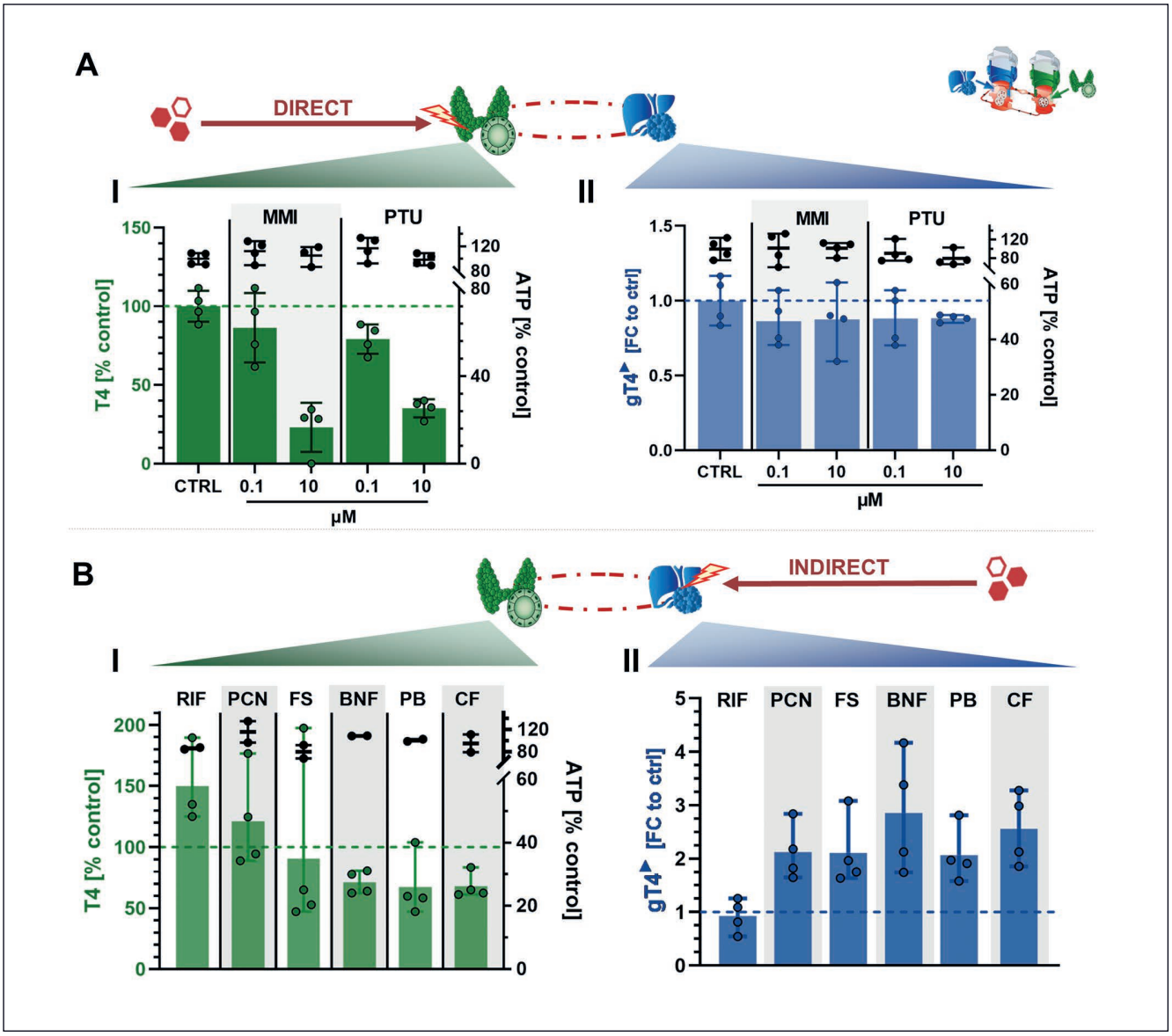

Fig. 7: Liver-thyroid co-cultivation allows detection and differentiation of direct as well as indirect thyroid effects in a single approach

(A) Co-culture was treated every 2 days for 4 days with compounds directly targeting thyroid function (TPO inhibitors; MMI, PTU). The medium was supplemented with 1 μM labeled T4 (T4▶). Culture supernatants were analyzed for thyroidal T4 secretion (green) and hepatic enzymatic formation of labeled T4 glucuronide (gT4▶, blue) after 3, 5, and 7 days. (I) Thyroidal T4 (green) and ATP (grey) levels in % in co-culture relative to vehicle control (DMSO) after 4 days of treatment with different concentrations (0.01 μM and 10 μM) of MMI or PTU. The green dotted line indicates thyroidal T4 secretion of the vehicle control (100%). (II) Hepatic enzymatic formation of T4▶ glucuronide (gT4▶) (blue) and ATP (grey) ratios in co-culture after 4 days of exposure. Ratios were calculated as fold change (gT4▶) and percent relative to the solvent control. The blue dotted line indicates the hepatic formation of gT4 from the vehicle control (FC value = 1). (B) Co-culture was treated every 3 days for 6 days with inducers of liver biotransformation (RIF, PCN, FS, BNF, PB, and CF). The medium was supplemented with 1 μM labeled T4 (T4▶). Culture supernatants were analyzed for thyroidal T4 and hepatic formation of labeled T4 glucuronide (gT4▶) after 3 and 6 days. (I) Thyroidal T4 secretion levels (green) and ATP levels (grey, n = 1, 2 technical replicates) after 6 days of treatment relative to the vehicle control (CTRL; DMSO). The green dotted line indicates thyroidal T4 secretion of the vehicle control (100%) (II) gT4▶ formation after 3 and 6 days of treatment relative to vehicle control (DMSO). The blue dotted line indicates hepatic labeled gT4 formation of the vehicle control. Presented as pooled data from 2 independent experiments (2 technical replicates/experiment) as mean ± SD (n = 2). Liver cells were isolated from 1 animal per experiment (AE) and thyroid cells from 4 animals (AS) per experiment.

A direct species comparison of rats and humans *in vivo* is hardly possible for biocides and PPP due to the lack of clinical data (for obvious reasons). The interpretation of rodent assay data for human safety risk assessment requires a sound understanding of the mechanism underlying a molecule's interference with thyroid homeostasis but also demands knowledge about its translation to humans. In the absence of specific counterevidence, both direct and indirect mechanisms of TH impairment need to be regarded as human-relevant. Translation of liver-mediated (indirect) TH impairment observed in rodents is particularly challenging. Although TSH-mediated thyroid tumor formation in rats resulting from chronic liver enzyme induction is generally accepted to have little human relevance, the impact of such indirect-acting chemicals on maternal T4 reduction and, concomitantly, on the offspring's neurodevelopment is not clear (Hassan et al., 2017; O'Shaughnessy and Gilbert, 2020; Ramhøj et al., 2020). We have therefore aimed to develop a rat thyroid-liver chip for a simultaneous investigation of direct and indirect mechanisms of thyroid perturbation on organ-level functions. The combined application with a very similar human thyroid-liver model established in parallel (Kühnlenz et al., 2022) will allow identifying potential species differences.

Three-dimensional (3D) models are being increasingly used to create authentic tissue-specific phenotypes *in vitro*. In contrast to conventional 2D cultures, 3D models can achieve a higher degree of structural complexity and longevity. These features are essential to retaining thyroid functionality *in vitro*, as the synthesis and release of THs is complex and requires a defined 3D ovoid (follicular) structure and a correct polarization of thyrocytes (Rousset et al., 2000). Recent developments illustrate different approaches to rebuilding complex thyroid morphology and function *in vitro*, highlighting the relevance of an interplay between thyrocytes and extracellular matrix (Samimi et al., 2021). For example, Saito et al. (2018) and Deisenroth et al. (2020) successfully reconstructed thyroid follicles from isolated primary thyrocytes of mouse and human origin following Matrigel embedding. These follicles developed correct cell polarity and, importantly, were able to produce THs. Deisenroth et al. (2020) also demonstrated that their human 3D thyroid model allowed the recapitulation of chemical-induced TH disruption on a functional level (TH synthesis). Alternative approaches described a successful establishment of 3D thyroid *in vitro* cultures by isolation of intact follicles from tissue explants, i.e., from rat and porcine tissues. Again, the structural and functional integrity was maintained by embedding follicles in collagen or Matrigel (Denef et al., 1980; Gärtner et al., 1985; Khoruzhenko et al., 2021). However, to the best of our knowledge, no rat 3D thyroid *in vitro* model has previously been published in which chemical-induced perturbation of TH release could be demonstrated.

This study aimed to achieve serum-free long-term cultivation of functional rat thyroid follicles, embedded in collagen, in a commercial microfluidic platform, thereby striving to minimize the use of materials whose production is associated with pain and suffering for animals. The successfully established rat thyroid follicle culture remained viable and maintained a follicular architecture with correct cellular polarity for at least 14 days. Expression of characteristic basolateral and apical specific proteins, including ZO-1, ezrin, pendrin, MCT8, and thyroglobulin, evinced correct follicular polarization, similar to previous reports (Delmarcelle et al., 2014; Deisenroth et al., 2020; Khoruzhenko et al., 2021). Moreover, these rat follicle cultures restored their capability to synthesize and secrete THs, predominantly T4, in the presence of TSH. Despite an evident stimulating effect of TSH on the production and release of T4, unstimulated follicles also secreted some amounts of T4, especially during the first days of cultivation. This observation might be attributable to the gradual exhaustion of a reserve capacity proposed from the ability of thyroid follicles to store iodinated thyroglobulin in the colloid (Zoeller et al., 2007). Noteworthy, the currently achieved T4 concentrations of 2-6 nmol/L in the medium of TSH-stimulated rat follicles *in vitro* are considerably lower than the T4 levels found in rat serum *in vivo*, which range between 43-88 nmol/L (Bartsch et al., 2018). However, the ratio of thyroid tissue to medium volume in our *in vitro* culture, ~ 200 follicles in 0.4 mL medium, is much lower than the corresponding ratio of estimated 40,000 follicles (Hartoft-Nielsen et al., 2005) and 12 mL blood volume (Lee and Blaufox, 1985) in rats *in vivo*. Moreover, isolated thyroid follicles in *in vitro* culture may not necessarily reflect the same follicle distribution concerning size and activity as in the thyroid gland *in vivo* (Gérard et al., 2004).

Reduced production and secretion of THs is the main functional consequence of compound-induced direct thyroid perturbation, with inhibition of thyroid peroxidase (TPO) probably being the best-characterized underlying molecular initiating event (MIE) (Noyes et al., 2019). TPO executes an important step of TH biosynthesis, catalyzing the iodination of tyrosyl residues of thyroglobulin (Carvalho and Dupuy, 2017). In the current study, treatment of the rat thyroid model with non-cytotoxic concentrations of the TPO inhibitors MMI and PTU caused a clear and concentration-dependent reduction of THs in the culture medium. The determined inhibitory effect concentrations (IC50 values) of MMI (0.56 µM) and PTU (0.41 µM) were well in the range of values previously reported in TPO inhibition assays using rat thyroid microsomes (Paul et al., 2013, 2014). The herein described decline of T4 by 78% after treatment with 10 µM PTU and 85% after 5 µM MMI is further well in line with data from a recently published animal study in which treatments with MMI and PTU corresponding to serum concentrations of ~8 µM (1367 ng/mL) and ~5 µM (512 ng/mL) reduced glandular T4 by 77% and 91%, respectively (Hassan et al., 2020). Collectively, these data provide evidence of technical feasibility and proficiency to identify compound-induced direct thyroid perturbation on organ-level function *in vitro*.

The second important mechanism of compound-induced thyroid disruption is mediated by the liver, i.e., through the acceleration of hepatic TH clearance subsequent to induction of xenobiotic biotransformation (Sutcliffe and Harvey, 2015). Therefore, this study also aimed to explore possibilities to address this indirect type of thyroid disruption by *in vitro* testing. There is a growing variety of *in vitro* liver models available of which liver

spheroids, often composed of primary hepatocytes and primary non-parenchymal liver cells (NPCs), have been recognized for their stable, liver-specific phenotype and longevity (Bell et al., 2016; Chang et al., 2017; Kyffin et al., 2019; Cox et al., 2020; Li et al., 2020). Our rat liver model also utilized spheroids embedded in collagen, which during this study turned out to be a robust, versatile, and easy-to-use culture method, compatible with different cell culture systems including TissUse's Multi-Organ-Chip (MOC) platform. The rat liver model remained viable and maintained a hepatocellular phenotype for 21 days. This was demonstrated by the expression of MCT8, ZO-1, and MRP2, as well as by the stable production and release of albumin and urea, which is in line with previous reports on similar models (Kyffin et al., 2019). In addition, our rat liver model releases gT4 after L-thyroxine supplementation, reflecting its ability to catabolize TH. Interestingly, the model did not release detectable amounts of sT4, which may reflect rat liver TH catabolism *in vivo*, with glucuronidation rather than sulfation being the major route of TH degradation (Peeters and Visser, 2000; Mullur et al., 2014).

Xenobiotics can enhance the baseline T4 degradation in the liver (Brucker-Davis, 1998; Crofton, 2008). This has already been reproduced *in vitro* using 2D hepatocyte cultures (Jemnitz et al., 2000; Richardson et al., 2014), which however do not allow stable long-term cultivation. In the current study, the 3D rat liver chip responded to a set of prototypical liver enzyme inducers not only by increasing the activities of CYP450 isoenzymes but also by increasing the level of gT4 in the culture medium. Overall these findings are consistent with corresponding *in vivo* data showing significantly enhanced gT4 formation in rats following the administration of chemicals like PCN or BNF (Saito et al., 1991; Barter and Klaassen, 1992; Viollon-Abadie et al., 1999; Klaassen and Hood, 2001; Richardson and Klaassen, 2010). Moreover, the individual compounds induced different effect patterns including clear evidence of a known species-specific induction of CYP3A1 by RIF and PCN (Lu and Li, 2001; Li et al., 2009). Interestingly, PCN, which strongly induced liver enzyme activity in the rat liver model, did not induce comparable effects in a similar human liver chip developed in parallel (Kühnlenz et al., 2022). In contrast, RIF induced CYP3A1 enzyme activity in the human liver model without increasing liver enzyme activity or gT4 formation in the rat liver model. This apparent "species tropism" of PCN and RIF has been observed previously (Kliewer et al., 1998; Jones et al., 2000). Together, results obtained in this rat liver chip document technical feasibility as well as proficiency to identify compound-induced indirect liver-mediated thyroid perturbation *in vitro* through quantification of gT4.

These promising data encouraged us to further pursue the next important goal of combining both models into one perfused rat thyroid-liver two-organ chip. We obtained a functional long-term co-culture model of rat thyroid and liver, maintaining key functions of both tissues, i.e., secretion of T4 from the thyroid component and release of albumin and urea from the liver component. This enabled us to investigate compound-induced direct and liver-mediated indirect thyroid perturbation in one single *in vitro* experiment. As the amounts of T4 released from the thyroid compartment (endogenous T4) were too low to demonstrate gT4 formation by the liver compartment, we decided to supplement the culture medium with labeled synthetic T4 (gT4$^{\blacktriangleright}$), enabling a concomitant and independent measurement of endogenous T4 and labeled gT4$^{\blacktriangleright}$.

In a final set of experiments, we exposed the rat thyroid-liver chip to non-cytotoxic concentrations of MMI and PTU, which caused a concentration-dependent decline of medium T4 without affecting the levels of gT4$^{\blacktriangleright}$. In contrast, treatment with several indirectly acting microsomal enzyme inducers enhanced levels of gT4$^{\blacktriangleright}$ in the medium. Some of these compounds also tended to reduce the medium levels of endogenous T4, evidently without inducing cytotoxicity in the thyroid model. Presumably, this drop in endogenous T4 levels results from enhanced T4 clearance reflecting the evident induction of the liver metabolism and directly corresponds to the observed increased formation of gT4 from the supplemented labeled T4. This nicely illustrates some potential use cases of this rat thyroid-liver organ-chip platform, as it enables the identification of compounds disrupting thyroid homeostasis and allows insights into underlying mechanisms without a need for animal studies. In summary, this co-culture model indeed allowed parallel functional testing for potential treatment-related effects on thyroid-derived T4 and liver-mediated gT4 formation, which appear most relevant for toxicological assessments.

In conclusion, this is the first time that a functional *in vitro* model combination of rat thyroid and liver tissue has been established successfully. At its current stage, the thyroid-liver organ chip demonstrates the feasibility of simultaneously capturing direct and indirect mechanisms of thyroid perturbation on a functional level *in vitro*. Furthermore, this model, in conjunction with a very similar human thyroid-liver model established in parallel (Kühnlenz et al., 2022), allows to directly test and investigate potential species differences between rat and human thyroid disruption in response to compound treatment. Notwithstanding, further efforts are needed to optimize and qualify the established model prior to being taken into consideration for initial chemical screening in a regulatory context.

Prospectively, we envision an application of the rat and human thyroid-liver chips to support a quantitative *in vitro* to *in vivo* extrapolation (QIVIVE). Given the historical *in vivo* data, the rat *in vitro* model can harness the potential to establish *in vitro* to *in vivo* correspondence in agreement with the 3R (replace, reduce, refine) concept. Through combination with approaches like toxicity-based toxicokinetic/toxicodynamic (TBTK/TD) modelling, the use of this type of *in vitro* organ-level function further maximizes and improves a data-driven and evidence-based human safety risk assessment.

References

Andersson, N., Arena, M., Auteri, D. et al. (2018). Guidance for the identification of endocrine disruptors in the context of Regulations (EU) No 528/2012 and (EC) No 1107/2009. *EFSA J 16*, e05311. doi:10.2903/j.efsa.2018.5311

Baker, M. (2016). Reproducibility: Respect your cells! *Nature 537*, 433-435. doi:10.1038/537433a

Bale, S. S., Geerts, S., Jindal, R. et al. (2016). Isolation and co-culture of rat parenchymal and non-parenchymal liver cells to evaluate cellular interactions and response. *Sci Rep 6*, 25329. doi:10.1038/srep25329

Barter, R. A. and Klaassen, C. D. (1992). Rat liver microsomal UDP-glucuronosyltransferase activity toward thyroxine: Characterization, induction, and form specificity. *Toxicol Appl Pharmacol 115*, 261-267. doi:10.1016/0041-008X(92)90331-L

Bartsch, R., Brinkmann, B., Jahnke, G. et al. (2018). Human relevance of follicular thyroid tumors in rodents caused by non-genotoxic substances. *Regul Toxicol Pharmacol 98*, 199-208. doi:10.1016/j.yrtph.2018.07.025

Beck-Peccoz, P., Persani, L., Calebiro, D. et al. (2006). Syndromes of hormone resistance in the hypothalamic-pituitary-thyroid axis. *Best Pract Res Clin Endocrinol Metab 20*, 529-546. doi:10.1016/j.beem.2006.11.001

Bell, C. C., Hendriks, D. F. G., Moro, S. M. L. et al. (2016). Characterization of primary human hepatocyte spheroids as a model system for drug-induced liver injury, liver function and disease. *Sci Rep 6*, 25187. doi:10.1038/srep25187

Berbel, P., Mestre, J. L., Santamaría, A. et al. (2009). Delayed neurobehavioral development in children born to pregnant women with mild hypothyroxinemia during the first month of gestation: The importance of early iodine supplementation. *Thyroid 19*, 511-519. doi:10.1089/thy.2008.0341

Bergman, Å., Heindel, J. J., Jobling, S. et al. (2013). *State of the Science of Endocrine Disrupting Chemicals 2012*. World Health Organization.

Brewer, C., Yeager, N. and Cristofano, A. D. (2007). Thyroid-stimulating hormone – Initiated proliferative signals converge in vivo on the mTOR kinase without activating AKT. *Cancer Res 67*, 8002-8006. doi:10.1158/0008-5472.CAN-07-2471

Brucker-Davis, F. (1998). Effects of environmental synthetic chemicals on thyroid function. *Thyroid 8*, 827-856. doi:10.1089/thy.1998.8.827

Caballero, M. V., Ares, I., Martínez, M. et al. (2015). Fipronil induces CYP isoforms in rats. *Food Chem Toxicol 83*, 215-221. doi:10.1016/j.fct.2015.06.019

Capen, C. C. (1994). Mechanisms of chemical injury of thyroid gland. *Prog Clin Biol Res 387*, 173-191.

Carvalho, D. P. and Dupuy, C. (2017). Thyroid hormone biosynthesis and release. *Mol Cell Endocrinol 458*, 6-15. doi:10.1016/j.mce.2017.01.038

Chang, S.-Y., Voellinger, J. L., Van Ness, K. P. et al. (2017). Characterization of rat or human hepatocytes cultured in microphysiological systems (MPS) to identify hepatotoxicity. *Toxicol In Vitro 40*, 170-183. doi:10.1016/j.tiv.2017.01.007

Cox, C. R., Lynch, S., Goldring, C. et al. (2020). Current perspective: 3D spheroid models utilizing human-based cells for investigating metabolism-dependent drug-induced liver injury. *Front Med Technol 2*, 611913. doi:10.3389/fmedt.2020.611913

Crivellente, F., Hart, A., Hernandez-Jerez, A. F. et al. (2019). Establishment of cumulative assessment groups of pesticides for their effects on the thyroid. *EFSA J 17*, e05801. doi:10.2903/j.efsa.2019.5801

Crofton, K. M. (2008). Thyroid disrupting chemicals: Mechanisms and mixtures. *Int J Androl 31*, 209-223. doi:10.1111/j.1365-2605.2007.00857.x

Deisenroth, C., Soldatow, V. Y., Ford, J. et al. (2020). Development of an in vitro human thyroid microtissue model for chemical screening. *Toxicol Sci 174*, 63-78. doi:10.1093/toxsci/kfz238

Dellarco, V. L., McGregor, D., Berry, S. C. et al. (2006). Thiazopyr and thyroid disruption: Case study within the context of the 2006 IPCS human relevance framework for analysis of a cancer mode of action. *Crit Rev Toxicol 36*, 793-801. doi:10.1080/10408440600975242

Delmarcelle, A.-S., Villacorte, M., Hick, A.-C. et al. (2014). An ex vivo culture system to study thyroid development. *J Vis Exp 6*, e51641. doi:10.3791/51641

Denef, J.-F., Björkman, U. and Ekholm, R. (1980). Structural and functional characteristics of isolated thyroid follicles. *J Ultrastruct Res 71*, 185-202. doi:10.1016/S0022-5320(80)90106-9

Desai, P. K., Tseng, H. and Souza, G. R. (2017). Assembly of hepatocyte spheroids using magnetic 3D cell culture for CYP450 inhibition/induction. *Int J Mol Sci 18*, 1085. doi:10.3390/ijms18051085

Dybing and Sanner (1999). Consensus Report: Species differences in chemical carcinogenesis of the thyroid gland, kidney and urinary bladder. In Capen, C. C., Dybing, E., Rice, J. M. (eds), *Species difference in thyroid, kidney and urinary bladder carcinogenesis*. *IARC Sci Publ 147*, 1-14. Lyon: IARC. https://bit.ly/3gOaCU0

Dovrtelova, G., Zendulka, O., Noskova, K. et al. (2018). Effect of endocannabinoid oleamide on rat and human liver cytochrome P450 enzymes in in vitro and in vivo models. *Drug Metab Dispos 46*, 913-923. doi:10.1124/dmd.117.079582

ECHA – European Chemicals Agency (2017). Guidance on the application of the CLP criteria: Guidance to Regulation (EC) No 1272/2008 on classification, labelling and packaging (CLP) of substances and mixtures. LU: Publications Office. https://data.europa.eu/doi/10.2823/124801 (accessed 08.04.2021)

ECHA (2021). Propylthiouracil – Substance Information – ECHA. https://echa.europa.eu/de/substance-information/-/substanceinfo/100.000.095 (accessed 23.05.2021)

EU (2009). Regulation (EC) No 1107/2009 of the European Parliament and of the Council of 21 October 2009 concerning the placing of plant protection products on the market and repealing Council Directives 79/117/EEC and 91/414/EEC. *OJ L 309*, 1-50. http://data.europa.eu/eli/reg/2009/1107/oj

EU (2012). Regulation (EU) No 528/2012 of the European Parliament and of the Council of 22 May 2012 concerning the making available on the market and use of biocidal products. *OJ L 167*, 1-123. http://data.europa.eu/eli/reg/2012/528/oj

European Chemical Agency (ECHA) and European Food Safety Authority (EFSA) with the technical support of the Joint Research Centre (JRC), Andersson, N., Arena, M. et al. (2018). Guidance for the identification of endocrine disruptors in the context of Regulations (EU) No 528/2012 and (EC) No 1107/2009. *EFSA J 16*, e05311. doi:10.2903/j.efsa.2018.5311

Foster, J. R., Tinwell, H. and Melching-Kollmuss, S. (2021). A review of species differences in the control of, and response to, chemical-induced thyroid hormone perturbations leading to thyroid cancer. *Arch Toxicol 95*, 807-836. doi:10.1007/s00204-020-02961-6

Gärtner, R., Greil, W., Stübner, D. et al. (1985). Preparation of porcine thyroid follicles with preserved polarity: Functional and morphological properties in comparison to inside-out follicles. *Mol Cell Endocrinol 40*, 9-16. doi:10.1016/0303-7207(85)90152-2

Gérard, A.-C., Denef, J.-F., Colin, I. M. et al. (2004). Evidence for processing of compact insoluble thyroglobulin globules in relation with follicular cell functional activity in the human and the mouse thyroid. *Eur J Endocrinol 150*, 73-80. doi:10.1530/eje.0.1500073

Ghassabian, A., El Marroun, H., Peeters, R. P. et al. (2014). Downstream effects of maternal hypothyroxinemia in early pregnancy: Nonverbal IQ and brain morphology in school-age children. *J Clin Endocrinol Metab 99*, 2383-2390. doi:10.1210/jc.2013-4281

Gilbert, M. E., Hassan, I., Wood, C. et al. (2022). Gestational exposure to perchlorate in the rat: Thyroid hormones in fetal thyroid gland, serum, and brain. *Toxicol Sci 188*, 117-130. doi:10.1093/toxsci/kfac038

Haddow, J. E., Palomaki, G. E., Allan, W. C. et al. (1999). Maternal thyroid deficiency during pregnancy and subsequent neuropsychological development of the child. *N Engl J Med 341*, 549-555. doi:10.1056/NEJM199908193410801

Hallinger, D. R., Murr, A. S., Buckalew, A. R. et al. (2017). Development of a screening approach to detect thyroid disrupting chemicals that inhibit the human sodium iodide symporter (NIS). *Toxicol Vitro 40*, 66-78. doi:10.1016/j.tiv.2016.12.006

Hariparsad, N., Ramsden, D., Palamanda, J. et al. (2017). Considerations from the IQ induction working group in response to drug-drug interaction guidance from regulatory agencies: Focus on downregulation, CYP2C induction, and CYP2B6 positive control. *Drug Metab Dispos 45*, 1049-1059.

Hartoft-Nielsen, M., Rasmussen, Å., Feldt-Rasmussen, U. et al. (2005). Estimation of number of follicles, volume of colloid and inner follicular surface area in the thyroid gland of rats. *J Anat 207*, 117-124. doi:10.1111/j.1469-7580.2005.00442.x

Hassan, I., El-Masri, H., Kosian, P. A. et al. (2017). Neurodevelopment and thyroid hormone synthesis inhibition in the rat: Quantitative understanding within the adverse outcome pathway framework. *Toxicol Sci 160*, 57-73. doi:10.1093/toxsci/kfx163

Hassan, I., El-Masri, H., Ford, J. et al. (2020). Extrapolating in vitro screening assay data for thyroperoxidase inhibition to predict serum thyroid hormones in the rat. *Toxicol Sci 173*, 280-292. doi:10.1093/toxsci/kfz227

Hurley, P. M. (1998). Mode of carcinogenic action of pesticides inducing thyroid follicular cell tumors in rodents. *Environ Health Perspect 106*, 437-445. doi:10.1289/ehp.98106437

Ito, O., Nakamura, Y., Tan, L. et al. (2006). Expression of cytochrome P-450 4 enzymes in the kidney and liver: Regulation by PPAR and species-difference between rat and human. *Mol Cell Biochem 284*, 141-148. doi:10.1007/s11010-005-9038-x

Jemnitz, K., Veres, Z., Monostory, K. et al. (2000). Glucuronidation of thyroxine in primary monolayer cultures of rat hepatocytes: In vitro induction of UDP-glucuronosyltranferases by methylcholanthrene, clofibrate, and dexamethasone alone and in combination. *Drug Metab Dispos 28*, 34-37.

Joannard, F., Galisteo, M., Corcos, L. et al. (2000). Regulation of phenobarbital-induction of CYP2B and CYP3A genes in rat cultured hepatocytes: Involvement of several serine/threonine protein kinases and phosphatases. *Cell Biol Toxicol 16*, 325-337. doi:10.1023/a:1026702615125

Jones, S. A., Moore, L. B., Shenk, J. L. et al. (2000). The pregnane X receptor: A promiscuous xenobiotic receptor that has diverged during evolution. *Mol Endocrinol 14*, 27-39. doi:10.1210/mend.14.1.0409

Kapałczyńska, M., Kolenda, T., Przybyła, W. et al. (2018). 2D and 3D cell cultures – A comparison of different types of cancer cell cultures. *Arch Med Sci 14*, 910-919. doi:10.5114/aoms.2016.63743

Khoruzhenko, A., Miot, F., Massart, C. et al. (2021). Functional model of rat thyroid follicles cultured in Matrigel. *Endocr Connect 10*, 570-578. doi:10.1530/EC-21-0169

Klaassen, C. D. and Hood, A. M. (2001). Effects of microsomal enzyme inducers on thyroid follicular cell proliferation and thyroid hormone metabolism. *Toxicol Pathol 29*, 34-40. doi:10.1080/019262301301418838

Kliewer, S. A., Moore, J. T., Wade, L. et al. (1998). An orphan nuclear receptor activated by pregnanes defines a novel steroid signaling pathway. *Cell 92*, 73-82. doi:10.1016/S0092-8674(00)80900-9

Kocarek, T. A., Schuetz, E. G., Strom, S. C. et al. (1995). Comparative analysis of cytochrome P4503A induction in primary cultures of rat, rabbit, and human hepatocytes. *Drug Metab Dispos 23*, 415-421.

Kooistra, L., Crawford, S., van Baar, A. L. et al. (2006). Neonatal effects of maternal hypothyroxinemia during early pregnancy. *Pediatrics 117*, 161-167. doi:10.1542/peds.2005-0227

Korevaar, T. I. M., Muetzel, R., Medici, M. et al. (2016). Association of maternal thyroid function during early pregnancy with offspring IQ and brain morphology in childhood: A population-based prospective cohort study. *Lancet Diabetes Endocrinol 4*, 35-43. doi:10.1016/S2213-8587(15)00327-7

Kühnlenz, J., Karwelat, D., Steger-Hartmann, T. et al. (2022). A microfluidic thyroid-liver platform to assess chemical safety in humans. *ALTEX*, online ahead of print. doi:10.14573/altex.2108261

Kyffin, J. A., Sharma, P., Leedale, J. et al. (2019). Characterisa-

tion of a functional rat hepatocyte spheroid model. *Toxicol In Vitro 55*, 160-172. doi:10.1016/j.tiv.2018.12.014

Lee, H. B. and Blaufox, M. D. (1985). Blood volume in the rat. *J Nucl Med 26*, 72-76.

Levie, D., Korevaar, T. I. M., Bath, S. C. et al. (2018). Thyroid function in early pregnancy, child IQ, and autistic traits: A meta-analysis of individual participant data. *J Clin Endocrinol Metab 103*, 2967-2979. doi:10.1210/jc.2018-00224

Lewandowski, T. A., Seeley, M. R. and Beck, B. D. (2004). Interspecies differences in susceptibility to perturbation of thyroid homeostasis: A case study with perchlorate. *Regul Toxicol Pharmacol 39*, 348-362. doi:10.1016/j.yrtph.2004.03.002

Li, F., Cao, L., Parikh, S. et al. (2020). Three-dimensional spheroids with primary human liver cells and differential roles of Kupffer cells in drug-induced liver injury. *J Pharm Sci 109*, 1912-1923. doi:10.1016/j.xphs.2020.02.021

Li, Y., Ross-Viola, J. S., Shay, N. F. et al. (2009). Human CYP3A4 and murine Cyp3A11 are regulated by equol and genistein via the pregnane X receptor in a species-specific manner. *J Nutr 139*, 898-904. doi:10.3945/jn.108.103572

Lu, C. and Di, L. (2020). In vitro and in vivo methods to assess pharmacokinetic drug-drug interactions in drug discovery and development. *Biopharm Drug Dispos 41*, 3-31. doi:10.1002/bdd.2212

Lu, C. and Li, A. P. (2001). Species comparison in P450 induction: Effects of dexamethasone, omeprazole, and rifampin on P450 isoforms 1A and 3A in primary cultured hepatocytes from man, Sprague-Dawley rat, minipig, and beagle dog. *Chem Biol Interact 134*, 271-281. doi:10.1016/s0009-2797(01)00162-4

Marty, S., Beekhuijzen, M., Charlton, A. et al. (2021). Towards a science-based testing strategy to identify maternal thyroid hormone imbalance and neurodevelopmental effects in the progeny – Part II: How can key events of relevant adverse outcome pathways be addressed in toxicological assessments? *Crit Rev Toxicol 51*, 328-358. doi:10.1080/10408444.2021.1910625

Meek, M. E. B., Bucher, J. R., Cohen, S. M. et al. (2003). A framework for human relevance analysis of information on carcinogenic modes of action. *Crit Rev Toxicol 33*, 591-653. doi:10.1080/713608373

Modesto, T., Tiemeier, H., Peeters, R. P. et al. (2015). Maternal mild thyroid hormone insufficiency in early pregnancy and attention-deficit / hyperactivity disorder symptoms in children. *JAMA Pediatr 169*, 838-845. doi:10.1001/jamapediatrics.2015.0498

Mullur, R., Liu, Y.-Y. and Brent, G. A. (2014). Thyroid hormone regulation of metabolism. *Physiol Rev 94*, 355-382. doi:10.1152/physrev.00030.2013

Noyes, P. D., Friedman, K. P., Browne, P. et al. (2019). Evaluating chemicals for thyroid disruption: Opportunities and challenges with in vitro testing and adverse outcome pathway approaches. *Environ Health Perspect 127*, 95001. doi:10.1289/EHP5297

OECD (2014). OECD Guideline for the Testing of Checmicals. 29 July 2014. Draft Proposal for a New Performance Based Test Guideline – Human cytochrome P450 (CYP) n-fold induction in vitro test method.

OECD (2018). Revised Guidance Document 150 on Standardised Test Guidelines for Evaluating Chemicals for Endocrine Disruption. *OECD Series on Testing and Assessment, No. 150*. OECD Publishing, Paris. https://www.oecd-ilibrary.org/content/publication/9789264304741-en

Oredsson, S., Coecke, S., van der Valk, J. et al. (2019). What is understood by "animal-free research"? *Toxicol In Vitro 57*, 143-144. doi:10.1016/j.tiv.2019.03.001

O'Shaughnessy, K. L. and Gilbert, M. E. (2020). Thyroid disrupting chemicals and developmental neurotoxicity – New tools and approaches to evaluate hormone action. *Mol Cell Endocrinol 518*, 110663. doi:10.1016/j.mce.2019.110663

Paul Friedman, K., Watt, E. D., Hornung, M. W. et al. (2016). Tiered high-throughput screening approach to identify thyroperoxidase inhibitors within the ToxCast Phase I and II chemical libraries. *Toxicol Sci 151*, 160-180. doi:10.1093/toxsci/kfw034

Paul, K. B., Hedge, J. M., Macherla, C. et al. (2013). Cross-species analysis of thyroperoxidase inhibition by xenobiotics demonstrates conservation of response between pig and rat. *Toxicology 312*, 97-107. doi:10.1016/j.tox.2013.08.006

Paul, K. B., Hedge, J. M., Rotroff, D. M. et al. (2014). Development of a thyroperoxidase inhibition assay for high-throughput screening. *Chem Res Toxicol 27*, 387-399. doi:10.1021/tx400310w

Peeters, R. P. and Visser, T. J. (2000). Metabolism of thyroid hormone. In K. R. Feingold, B. Anawalt, A. Boyce et al. (eds), *Thyroid Disease Manager*. Chapter 5. Endotext [Internet]. South Dartmouth, MA, USA: MDText.com, Inc. http://www.ncbi.nlm.nih.gov/books/NBK285545/ (accessed 02.03.2021)

Punt, A., Bouwmeester, H., Blaauboer, B. J. et al. (2020). New approach methodologies (NAMs) for human-relevant biokinetics predictions: Meeting the paradigm shift in toxicology towards an animal-free chemical risk assessment. *ALTEX 37*, 607-622. doi:10.14573/altex.2003242

Raasch, M., Fritsche, E., Kurtz, A. et al. (2019). Microphysiological systems meet hiPSC technology – New tools for disease modeling of liver infections in basic research and drug development. *Adv Drug Deliv Rev 140*, 51-67. doi:10.1016/j.addr.2018.06.008

Ramhøj, L., Hass, U., Gilbert, M. E. et al. (2020). Evaluating thyroid hormone disruption: Investigations of long-term neurodevelopmental effects in rats after perinatal exposure to perfluorohexane sulfonate (PFHxS). *Sci Rep 10*, 2672. doi:10.1038/s41598-020-59354-z

Richardson, T. A. and Klaassen, C. D. (2010). Disruption of thyroid hormone homeostasis in Ugt1a-deficient Gunn rats by microsomal enzyme inducers is not due to enhanced thyroxine glucuronidation. *Toxicol Appl Pharmacol 248*, 38-44. doi:10.1016/j.taap.2010.07.010

Richardson, V. M., Ferguson, S. S., Sey, Y. M. et al. (2014). In vitro metabolism of thyroxine by rat and human hepatocytes.

Xenobiotica 44, 391-403. doi:10.3109/00498254.2013.847990

Roques, B. B., Lacroix, M. Z., Puel, S. et al. (2012). CYP450-dependent biotransformation of the insecticide fipronil into fipronil sulfone can mediate fipronil-induced thyroid disruption in rats. *Toxicol Sci 127*, 29-41. doi:10.1093/toxsci/kfs094

Roques, B. B., Leghait, J., Lacroix, M. Z. et al. (2013). The nuclear receptors pregnane X receptor and constitutive androstane receptor contribute to the impact of fipronil on hepatic gene expression linked to thyroid hormone metabolism. *Biochem Pharmacol 86*, 997-1039. doi:10.1016/j.bcp.2013.08.012

Rousset, B., Dupuy, C., Miot, F. et al. (2000). Thyroid hormone synthesis and secretion. In K. R. Feingold, B. Anawalt, A. Boyce et al. (eds),. *Thyroid Disease Manager.* Chapter 2. Endotext [Internet]. South Dartmouth, MA, USA: MDText.com, Inc. http://www.ncbi.nlm.nih.gov/books/NBK285550/ (accessed 03.06.2021)

Saito, K., Kaneko, H., Sato, K. et al. (1991). Hepatic UDP-glucuronyltransferase(s) activity toward thyroid hormones in rats: Induction and effects on serum thyroid hormone levels following treatment with various enzyme inducers. *Toxicol Appl Pharmacol 111*, 99-106. doi:10.1016/0041-008X(91)90138-5

Saito, Y., Onishi, N., Takami, H. et al. (2018). Development of a functional thyroid model based on an organoid culture system. *Biochem Biophys Res Commun 497*, 783-789. doi:10.1016/j.bbrc.2018.02.154

Samimi, H., Atlasi, R., Parichehreh-Dizaji, S. et al. (2021). A systematic review on thyroid organoid models: Time-trend and its achievements. *Am J Physiol-Endocrinol Metab 320*, E581-E590. doi:10.1152/ajpendo.00479.2020

Santini, F., Vitti, P., Ceccarini, G. et al. (2003). In vitro assay of thyroid disruptors affecting TSH-stimulated adenylate cyclase activity. *J Endocrinol Invest 26*, 950-955. doi:10.1007/BF03348190

Schröder-van der Elst, J. P., van der Heide, D., Romijn, J. A. et al. (2004). Differential effects of natural flavonoids on growth and iodide content in a human Na^+/I^- symporter-transfected follicular thyroid carcinoma cell line. *Eur J Endocrinol 150*, 557-564. doi:10.1530/eje.0.1500557

Singh, G. and Correa, R. (2021). Methimazole. In *StatPearls*. Treasure Island, FL, USA: StatPearls Publishing. http://www.ncbi.nlm.nih.gov/books/NBK545223/ (accessed 23.05.2021)

Sutcliffe, C. and Harvey, P. W. (2015). Chapter 11 – Endocrine disruption of thyroid function: Chemicals, mechanisms, and toxicopathology. In P. D. Darbre (ed.), *Endocrine Disruption and Human Health* (201-217). Boston, USA: Academic Press. doi:10.1016/B978-0-12-801139-3.00011-9

Vansell, N. R. and Klaassen, C. D. (2002). Increase in rat liver UDP-glucuronosyltransferase mRNA by microsomal enzyme inducers that enhance thyroid hormone glucuronidation. *Drug Metab Dispos 30*, 240-246. doi:10.1124/dmd.30.3.240

Vansell, N. R., Muppidi, J. R., Habeebu, S. M. et al. (2004). Promotion of thyroid tumors in rats by pregnenolone-16α-carbonitrile (PCN) and polychlorinated biphenyl (PCB). *Toxicol Sci 81*, 50-59. doi:10.1093/toxsci/kfh197

Viollon-Abadie, C., Lassere, D., Debruyne, E. et al. (1999). Phenobarbital, β-naphthoflavone, clofibrate, and pregnenolone-16α-carbonitrile do not affect hepatic thyroid hormone UDP-glucuronosyl transferase activity, and thyroid gland function in mice. *Toxicol Appl Pharmacol 155*, 1-12. doi:10.1006/taap.1998.8558

Wang, J., Hallinger, D. R., Murr, A. S. et al. (2018). High-throughput screening and quantitative chemical ranking for sodium-iodide symporter inhibitors in ToxCast phase I chemical library. *Environ Sci Technol 52*, 5417-5426. doi:10.1021/acs.est.7b06145

Wikswo, J. P. (2014). The relevance and potential roles of microphysiological systems in biology and medicine. *Exp Biol Med (Maywood) 239*, 1061-1072. doi:10.1177/1535370214542068

Zoeller, R. T., Tan, S. W. and Tyl, R. W. (2007). General background on the hypothalamic-pituitary-thyroid (HPT) axis. *Crit Rev Toxicol 37*, 11-53. doi:10.1080/10408440601123446

Conflict of interest

Uwe Marx is shareholder and CSO of TissUse GmbH, which commercializes MPS platforms. All other authors declare that they have no conflict of interest.

Data availability

The research data that are not included in the article are available upon request from the corresponding author.

Acknowledgement

This work was funded by Bayer AG through a Life Science Collaboration program.